The fate of stars born in gas-rich high redshift galaxies

Floor van Donkelaar

Lund Observatory
Lund University

2021-EXA174

Degree project of 60 higher education credits (for a degree of Master)
May 2021

Supervisor: Oscar Agertz

Lund Observatory
Box 43
SE-221 00 Lund
Sweden

Abstract

In the early Universe, the Milky Way galaxy was considerably more gas-rich compared to today. In gas-rich galaxies, gravity and stellar feedback processes lead to significant levels of gas turbulence, with a more clumpy and irregular morphology, in contrast to well-ordered spiral structures that characterise local disk galaxies. Spectroscopic surveys of Milky Way's stars have revealed spatial, chemical, and kinematical structures that encode its assembly history. In the Milky Way, stars are observed to gather in two sequences, at high and low [α/Fe]. The high-[α/Fe] sequence broadly corresponds to old stars that are kinematically hot ($\sigma \geq 20$ km/s) and spatially distributed in a geometrically thick and radially compact disk. Whereas the younger low [α/Fe] stars tend to be kinematically colder ($\sigma \sim 10$ km/s) and reside in the geometrically thin disk. Furthermore, observations have revealed that thick disk stars feature a wide range of orbital eccentricities, while thin disk stars are better characterised by close to circular orbits.

It is well known that many physical mechanisms come into play during the evolution of galaxies, including mergers and secular processes such as heating by instabilities in the disk. In this work, we explore the possibility of the thin and thick disk kinematical properties being an outcome of purely in-situ mechanisms due to the gas-rich and turbulent environments in which stars form in the early Universe.

To address this problem, we carry out hydrodynamical+N-body simulations of entire galactic disks with gas fractions between 10 and 70 percent, and compare them to observational literature data from the APOGEE survey and Gaia. By doing so, we approximate the environmental conditions of the Milky Way's gas-rich past. We demonstrate stellar velocity dispersions ~ 30 km/s in newly born stars are generated by galaxies with a gas fraction $\geq 50\%$. We find that galaxies with an initial gas fraction of 30% have a vertical velocity dispersion that approximately marks the transition between the thin and thick disk. As such, the turbulent and fragmented interstellar medium at higher gas fractions act as a *barrier* against thin disk formation. A direct comparison to the Milky Way's age-velocity dispersion relation can be made by mapping the estimated redshift range of each simulation to the corresponding $\sigma_{\mathrm{z,birth}}$. From this, we determine that turbulent heating is a non-negligible part of the total stellar heating in a disk galaxy, being responsible for at least 30% of the heating at all time, and as much as 50% for stars older than 9 Gyr.

In a similar way, we find that stars born in disk galaxies with a 10% gas fraction feature stars on mostly circular orbits, with a mean orbital eccentricity less than 0.2. As the gas fraction is increased, more stars end up on more eccentric orbits. We find that once the gas fraction is $\gtrsim 30\%$, all eccentricity distributions are characterised by mean eccentricities of ~ 0.5, with more uniform distributions found for the highest gas fractions simulations. By combining the simulated eccentricity distributions with observational data, we infer the gas fractions and formation epochs of the Milky Way's chemically defined thick and thin disks. We find that both disks require some contribution of gas-rich and -poor regimes to fully retrieve their eccentricity distributions. However, most ($\sim 70\%$) of the thick disk was formed in a high gas fraction ($\geq 50\%$) environment, whereas 80% of the thin disk was formed in a low gas fraction ($\leq 20\%$) environment.

Keywords: Galaxies: Evolution - Galaxies: Kinematics and Dynamics - Methods: Numerical

Popular Summary

One of the greatest challenges astronomers are facing today is understanding how galaxies form. We know that the Milky Way is a spiral disk galaxy, similar to many others we see in the sky, therefore the Milky Way is a benchmark for understanding the inner workings of disk galaxies. The task of unraveling the mystery of the formation of the Milky Way has been given to astronomers, who attempt to construct models of the Galaxy's evolution based on its present appearance.

These models need to account for not only the large-scale gravitational forces involved in assembling the Galaxy, but also the chemical composition and motion of one of its primary components: the stars. It turns out that the chemistry and kinematics of the stars hold clues to how the Galaxy was made and how it has changed through time. Constraining the different properties of stars, one can subdivide the spiral disk of the Galaxy into a thin and thick disk. The thick disk mostly includes older stars that have a bigger spread in vertical velocity (= kinematically hot), whereas the thin disk has younger stars that have a smaller spread (= kinematically cold). *But how did these two disks form and why are they so different?*

There are multiple theories going around on how the thick disk has been formed. Some models assume a continuous evolutionary transition in the formation of the thick disk and the thin disk. Others believe that a component of the thick disk had its origin in a merger event where two galaxies collided. In this work we explored the possibility of the thin and thick disk properties to be formed in a simulation without any influence from outside the Galaxy.

When the Milky Way was younger it consisted of more gas, so stars had more opportunities to get kinematically hot by the turbulence of the gas. This leads to older stars having a higher velocity dispersion at birth than the stars born more recently, but also their orbital properties such as eccentricity change. Using simulations of Milky Way-like galaxies we calculated this birth velocity dispersion at different times in our galaxy's past. Many scientists focus on the secular heating, the physical process after the star is born where the star gets more kinematically hot due to interactions with gas clouds, spiral arms of the Galaxy etc., of the star to explain the difference between the thick and thin disk. In this project, we had another approach, and looked at the heating by the turbulence at birth.

In figure 1 we see the relationship between the birth velocity dispersion and age indicated by the black line, the gray area illustrates the margin of error of this relation. The colored blocks indicate different gas fraction environment the stars are born in. Using this figure we can see that turbulent heating plays a very big role in the general heating of older stars. There is relations between age and birth velocity dispersion, stars born in a higher gas fraction galaxy have a higher vertical velocity dispersion. Showing us that at least a part of the question: *"How did the different disks form?"*, can be answered using turbulent heating.

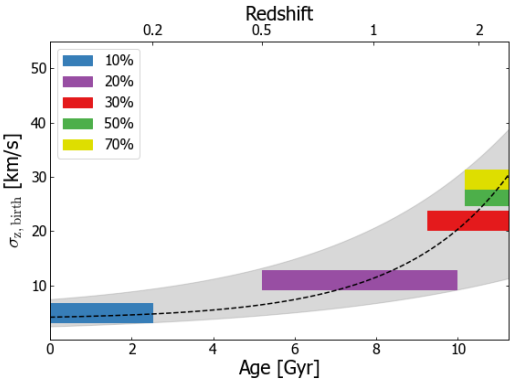

Figure 1: Age-birth velocity dispersion relation using different gas fraction simulations.

Samenvatting

Een van de grootste uitdagingen waarmee astronomen tegenwoordig worden geconfronteerd, is het begrijpen hoe sterrenstelsels ontstaan. We weten dat de Melkweg een spiraalvormig sterrenstelsel is, vergelijkbaar met vele anderen die we aan de hemel zien. De Melkweg is daarom een maatstaf voor het begrijpen van de innerlijke werking van sterrenstelsels in het algemeen. Astronomen proberen modellen te construeren van de evolutie van de Melkweg om zo het proces van vorming te ontrafelen.

Deze modellen moeten niet alleen rekening houden met de zwaartekracht, maar ook met de chemische samenstelling en beweging van de belangrijkste componenten: de sterren. Het blijkt dat deze eigenschappen aanwijzingen bevatten over hoe de Melkweg is onstaan en hoe deze in de loop van de tijd is veranderd. Door de verschillende eigenschappen van sterren te categoriseren, kan men de spiraalvormige schijf van de Melkweg verdelen in een dunne en dikke schijf. De dikke schijf bevat meestal oudere sterren en heeft een grotere snelheidsverspreiding, terwijl de dunne schijf uit jongere sterren bestaat die een kleinere verspreiding laten zien. *Maar hoe zijn deze twee schijven ontstaan?*

Er zijn verschillende theorieën over hoe de dikke schijf is onstaan. Sommige modellen gaan uit van een grote fusie van de Melkweg met een ander sterrenstelsel. In dit werk hebben we onderzocht of het mogelijk is de eigenschappen van dunne en dikke schijven na te bootsen zonder enige invloed van buitenaf.

Toen de Melkweg jonger was, bestond het uit meer gas, dus sterren hadden meer mogelijkheden om opgewarmd te worden door de door gas veroorzaakte turbulentie. Dit heeft ertoe geleid dat oudere sterren bij de geboorte een hogere snelheidsverspreiding hebben, maar ook dat hun radiale eigenschappen anders zijn. Met behulp van simulaties van Melkwegachtige sterrenstelsels hebben we deze geboortesnelheidsverspreiding op verschillende tijdstippen in het verleden van ons sterrenstelsel berekend. Veel wetenschappers richten zich op de seculiere verwarming van de ster, het fysieke proces waarbij de sterren meer snelheidverspreiding krijgen door interacties met bijvoorbeeld gaswolken, het verschil tussen de dikke en dunne schijf te verklaren. In dit project hebben we een andere benadering waar we kijken naar de verwarming door de turbulentie bij geboorte.

In figuur 2 is de relatie tussen de geboortesnelheidsverspreiding en de leeftijd te zien, het grijze gebied illustreert de foutmarge van deze relatie. De gekleurde blokken wijzen naar de verschillende gasfractie omgevingen waarin de sterren worden geboren in onze simulaties. Aan de hand van dit figuur kunnen we zien dat turbulente opwarming een zeer grote rol speelt bij de algemene opwarming van sterren. Sterren geboren in een sterrenstelsel met een hogere gasfractie hebben een grotere snelheidsverspreiding. We laten zien dat in ieder geval een deel van de vraag: *"Hoe zijn de verschillende schijven gevormd?*" kan worden beantwoord met turbulente opwarming.

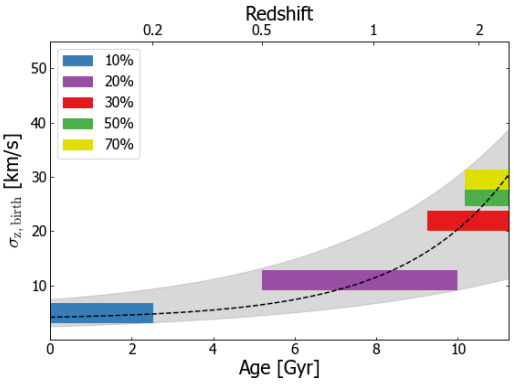

Figure 2: De relatie tussen de leeftijd en snelheidsverspreiding van sterren.

Contents

Chapter 1

Introduction & Theory

Understanding the formation and evolution of galaxies is a central theme in modern astrophysics. Our Galaxy, the Milky Way, is a benchmark for understanding disk galaxies. It is the only galaxy whose formation history can be studied using the full distribution of stars and thus provides us with a fundamental test site for theories of galaxy formation and evolution (Freeman & Bland-Hawthorn 2002). Next to using observational data, numerical simulations have become a primary tool for understanding and testing galaxy formation and evolution theories. The field has made significant progress over the last decade, for example, it is now possible to simulate the formation of individual galaxies and galaxy populations from well-defined initial conditions (Naab & Ostriker 2017).

Figure 1.1 shows the different structural components of the Milky Way. It consists of a bar-shaped core region surrounded by a disk of gas, dust, and stars. The Sun is located $\sim$ 7-9 kpc from the Galactic Center. In the inner few kiloparsecs is a dense concentration of mostly old stars in a roughly spheroidal distribution called the bulge (Freeman & Bland-Hawthorn 2002; Bland-Hawthorn & Gerhard 2016). Furthermore, it has been observed that stars gather in two sequences, at a high and low [α/Fe]. The high-[α/Fe] sequence broadly corresponds to old stars that are kinematically hot, with vertical velocity dispersions of $\sigma \geq 20$ km/s, and geometrically distributed in a thick and radially compact disk. In contrast, the younger low-[α/Fe] stars tend to be kinematically colder ($\sigma \sim 10$ km/s) and reside in the geometrically distributed thin disk (e.g. Holmberg et al. 2009; Mackereth et al. 2019). The disk is the defining stellar component of disk galaxies, and understanding its formation is a central goal of the galaxy formation theory.

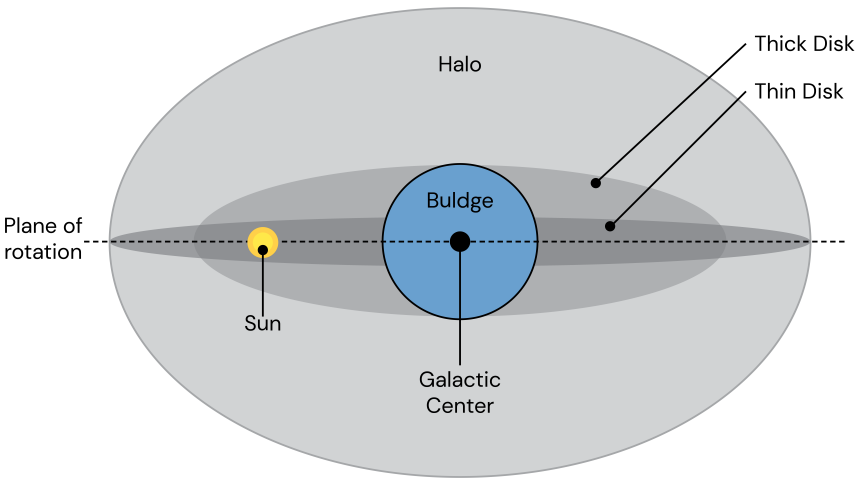

Figure 1.1: Depiction of the Milky Way showing the main stellar components, defined primarily by their spatial distributions.

Therefore, a key question is when different structural components of the galaxies were formed (van Dokkum et al. 2013).

The gas fraction of the Milky Way has been in decline since its formation (Santini et al. 2014). Furthermore, the stellar mass of the Milky Way has likely been increasing for the last 11 Gyrs as shown by (van Dokkum et al. 2013). More than half of the present-day mass of the Milky Way was assembled in the 3 Gyr period from z = 2.5 to z = 1. The stellar mass growth is likely dominated by the star formation at all redshifts, telling us that the globally averaged star formation rates (SFRs) is also in decline (Barnes et al. 2017).

In many ways, the Milky Way can been seen as the typical example of a large galaxy today in a low-density environment (Kormendy & Barentine 2010), especially when considering its global parameters, like the SFR, and given its total stellar mass (de Rossi et al. 2009). On the other hand, our Galaxy has probably not experienced a major merger for the past 10 Gyr indicating a quiet accretion history for a luminous galaxy (Stewart et al. 2008). Nevertheless, the Milky Way is an important benchmark for galaxy evolution because it provides information that cannot be obtained from extragalactic sources. In this work, we explore the possibility of the thin and thick disk kinematical properties in the Milky Way being an outcome of purely in situ mechanisms due to the gas-rich environments in which stars form in the early Universe .

1.1 Disk evolution and kinematics

Understanding the chemo-dynamical evolution of the Milky Way disk is a crucial step toward reconstructing the history of the Galaxy. Since the first works highlighting the existence of the Milky Way's thin and thick disk (Yoshii 1982; Gilmore & Reid 1983), research has been ongoing to find the structural and chemo-dynamical difference between the two disk populations (Recio-Blanco et al. 2014). The geometrically thin disk has a longer radial scalelength than the thick disk (Jurić et al. 2008). High-[α/Fe] stars are found to form a thicker, but more centrally concentrated component than low-[α/Fe] stars (Bovy et al. 2012; Hayden et al. 2015). Furthermore, the high-[α/Fe] stars are in general more radially compact (Bensby et al. 2014), older (Bensby et al. 2014; Feuillet et al. 2019), and kinematically hotter (e.g. Holmberg et al. 2009).

There is currently no consensus on the origin of the thick disk. Different theories for the origin of thick disks have been discussed and tested (e.g. Sales et al. 2009; Aumer et al. 2017). Amongst the scenarios proposed to explain the formation of the thick disk are the thickening of a pre-existing thin disk through a minor merger (e.g. Quinn et al. 1993; Villalobos & Helmi 2008), the direct accretion of stars from disrupted satellites (e.g. Abadi et al. 2003), the scattering or migration of stars by spiral arms (e.g. Schönrich & Binney 2009a,b), heating by giant molecular clouds (e.g. Aumer et al. 2016a) and in-situ triggered star formation after gas-rich mergers (e.g. Brook et al. 2005). More recent simulations demonstrate scenarios such as clumpy formation to form the high-[α/Fe] disk (e.g. Clarke et al. 2019; Debattista et al. 2019) or gas accretion to form the low-[α/Fe] sequence (Agertz et al. 2021; Buck et al. 2020).

While some of these scenarios predict a formation with the geometric thin disk significantly forming after the thick disk has formed, in other scenarios the thin disk is expected to start forming simultaneously with the thick disk, with the consequence that a significant population of old thin disk stars should exist (e.g. Beraldo e Silva et al. 2021). Using detailed analysis of the disk component of a simulated galaxy formed in the ΛCDM cosmogony, Abadi et al. (2003) found that $\sim$ 15% of the currently kinematically defined thin disk stars should have ages older than 10 Gyr, giving us strong evidence for some kind of co-formation of the disks. In an inside-out formation scenario, on the other hand, we expect them to form separately. In that case, the outer disk edge moves progressively from smaller to larger radii, due to the continuous formation of new stars in disk subpopulations of increasing scale-length (Bird et al. 2013). This scenario is the generic prediction of cosmological simulations of Milky Way-mass spiral galaxies (e.g. Abadi et al. 2003; Agertz et al. 2011; Brook et al. 2012) due to the steady buildup of

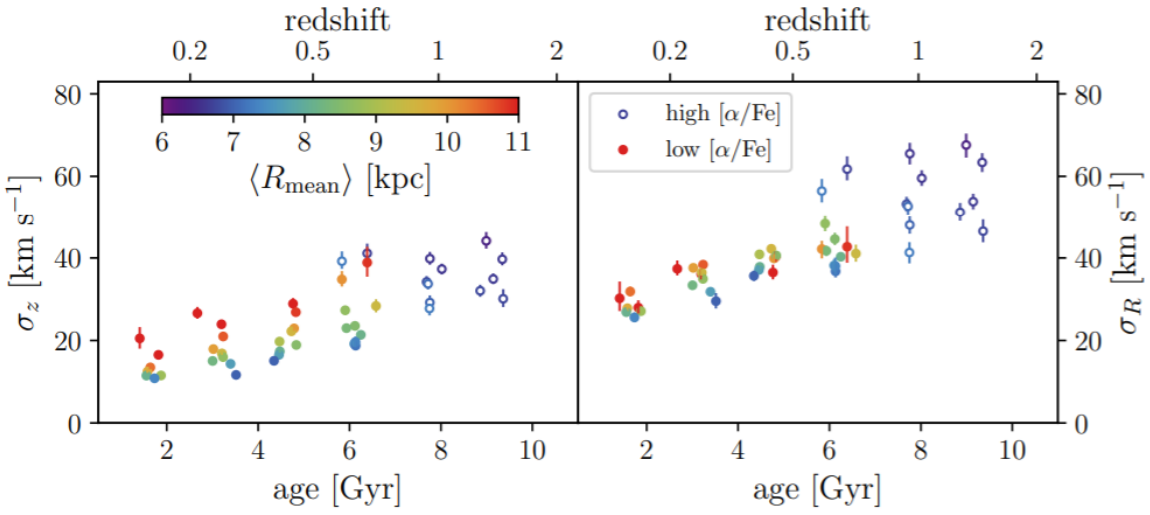

Figure 1.2: Vertical an radial velocity dispersions σ_z (left) and σ_R (right) from Mackereth et al. (2019) using the Gaia and APOGEE surveys. The points are coloured by the median of the mean orbital radius in each bin, to demonstrate the Galactocentric radius at which the stars reside. Furthermore the chemical thick (high [α/Fe]) and thin (low [α/Fe]) disk are indicated. The velocity dispersions increase with age of the stellar populations, with thick disc stars being kinematically hotter than co-eval thin disc stars formed $\sim 6-7$ Gyr ago.

angular momentum from large scale tidal torques coupled to a non-destructive contribution of accreting gas to the disk's angular momentum reservoir (Agertz et al. 2021).

For the first of these scenarios, heating due to a merger, the thick disk is predominantly the result of rapid heating of a pre-existing thin disk through one relatively massive merger event (Villalobos & Helmi 2008). In this scenario, a modest fraction of the original thin disk is preserved, and a small portion of present-day thick disk stars were formed in the satellite galaxy and are on highly eccentric orbits. In the accretion scenario, thick disk stars mostly form in an external satellite galaxy that gets disrupted while on an orbit near the disk plane. This can produce many properties of observed old thick disk components (see Abadi et al. 2003). The third scenario, radial migration, focuses on internal processes and proposes that the thick disk is created from stars migrating outwards from the kinematically hotter inner regions of the Milky Way (Schönrich & Binney 2009b) and in the fourth scenario the thick disk is the result of secular heating only. Finally, in the gas-rich merger scenario, a minor merger epoch brings gas into the galaxy from which thick disk stars form before the gas completely settles into a thin disk (Dierickx et al. 2010). This work will mainly focus on the fourth scenario, and to what degree strong interstellar turbulence can imprint large velocity dispersion in the stars.

1.1.1 Kinematical heating of stars

The velocity dispersion, σ, is an important property of a population of stars that can tell us a lot about its heating history over time. It is described as the statistical dispersion of velocities of the mean velocity of a group. A key observable diagnostic for the formation history of the Galaxy is the age–velocity dispersion relation (AVR), whose shape is intimately related to past kinematic heating events and processes. In the Milky Way, the vertical, σ_z, and radial, σ_R, velocity dispersions both increase roughly monotonically as a function of age, with σ_z going from $\sim$ 10 to $\sim$ 40 km/s and σ_R increasing from $\sim$ 30 to a maximum of $\sim$ 70 km/s in the oldest, high-[α/Fe] stellar populations (Bovy et al. 2016; Mackereth et al. 2019, see figure 1.2). The Geneva–Copenhagen survey demonstrated that the square of the vertical velocity dispersion increases linearly with age (Nordström et al. 2004) which indicates that more gradual, secular

heating processes play an important part in the disk evolution. Additionally, the measurement of AVRs and σ_z/σ_R across the disk from Mackereth et al. (2019) using Gaia and APOGEE data indicate that low-[α/Fe], inner disk stellar populations are likely dynamically heated by both giant molecular clouds (GMCs) and spiral arms, while the observed trends for outer disk populations require a significant contribution from another heating mechanism such as satellite perturbations. Spitzer & Schwarzschild (1953) showed that scattering of stars off small-scale irregularities in the potential of the galactic disk would lead to secular heating. The discovery of GMCs provided a new suitable candidate for the heating agent (Aumer et al. 2016a). Using analytic arguments, Lacey (1984) showed that GMC heating could have contributed significantly to the observed AVR. Furthermore, several N-body simulation studies have indicated that spiral arms and bars are efficient at increasing the velocity dispersion of stars in the planar direction (Sellwood & Carlberg 1984; Minchev & Quillen 2006), which can then be transformed into vertical motion from star scattering off GMCs or other massive bodies (Grand et al. 2016).

The AVR is typically described as a simple power-law in age $\sigma(t) \propto \tau^{\beta}$ with exponent β (Aumer & Binney 2009). With this type of relation, the velocity dispersion will increase with the age of stellar populations at all radii, meaning the traditional idea of a thick, old, and kinematically hot disk will be present. Aumer et al. (2016b) and Aumer et al. (2016a) showed that the observed radial and vertical AVRs are reproduced by models that lack a thick disk but have a thin disk and a dark halo with appropriate masses and the right quantity of GMCs. In contrary, the models in Aumer et al. (2017) and Aumer & Binney (2017) do show a thick disk; the thick disk stars are then created ad-hoc giving them a different birth velocity dispersion depended on when they were born. By doing this, the correlations between the vertical heating and the in-plane heating and migration could be missing. A clear relation between age and heating, including both the thin and thick stars, thus seems to be missing.

1.1.2 Orbital properties of thin and thick disks

It has long been understood that a star moving in the galactic potential will be subject to transient interactions with for example the galactic spiral arms and giant molecular clouds. These interactions generally have as an effect that initially circular orbits overtime become less circular, i.e. more eccentric, an effect often referred to as "blurring". Furthermore, stars can move from a circular orbit to another circular orbit and thus erasing all memory from the past kinematic history of the star. This is known as "churning" or radial migration. Radial migration is responsible for spreading stars away from their birth radius, this happens when stars are scattered by a non-axisymmetric structure such as a bar or a spiral arm, which can lead to their angular momentum changing (Sellwood & Binney 2002).

As discussed in section 1.1, radial migration is one of the possible theories on the formation of the thick disk. Schönrich & Binney (2009b) proposed that the chemical differentiation between thin and thick disks could be explained solely by radial migration, which might have brought stars with high vertical kinetic energy from the inner part of the Milky Way out to the Solar neighborhood. Whilst Vera-Ciro et al. (2014) found that migration will strongly affect the thin disk, but that it is not likely for the thick disk to be formed solely by radial migration.

There are more kinematical properties than just the velocity dispersion that separate the thin and thick disk, like the eccentricity of a star. The thin disk is characterized by stars on low-eccentricity orbits. In turn, the chemical thick disk has a high eccentricity tail and is thus more centrally concentrated and has a higher fraction of stars on eccentric orbits as is shown in figure 1.3 (adapted from Li et al. 2018). The eccentricity of a star is a parameter that determines the amount by which its orbit around another body deviates from a perfect circle, which can be calculated as follows

$$e = \frac{r_a - r_p}{r_a + r_p}, \tag{1.1}$$

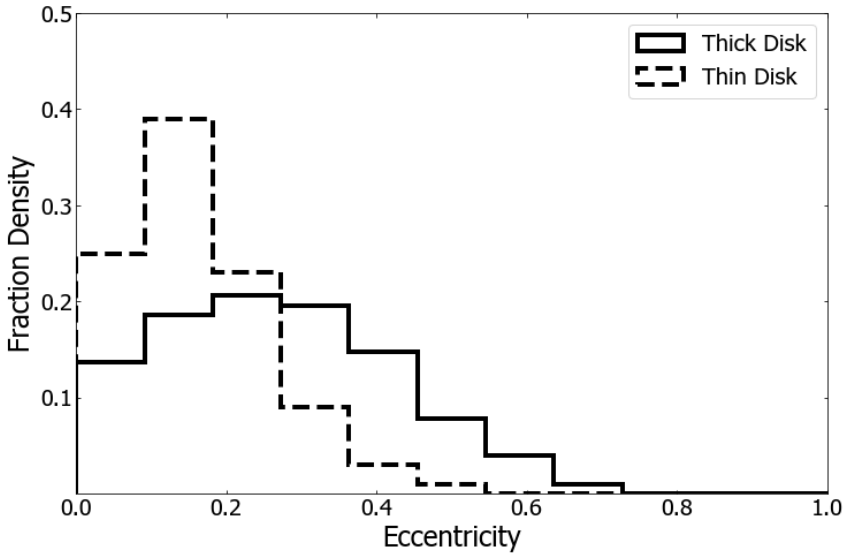

Figure 1.3: Distribution of the orbital eccentricity of the disk stars in the Milky Way Solar neighbourhood (adapted from Li et al. 2018) for the chemical defined thin (dashed line) and thick disk (solid line).

where r_a and r_p are the apocenter and pericenter radii of the stars. Sales et al. (2009) studied the orbital properties of stars in simulations of thick disks formed by the above-mentioned scenarios. They found that the distribution of orbital eccentricities are predicted to be different for each model. A prominent peak at low eccentricity is expected for the heating, migration, and gas-rich merging scenarios, while the eccentricity distribution is broader and shifted towards higher values for the gas accretion model. The accretion of gas onto the disk as a result of satellite mergers is most consistent with the observed distribution in the Milky Way.

Beraldo e Silva et al. (2021) used the eccentricity of old stars ($\tau > 10$ Gyr) within 2 kpc from the Sun as evidence for an early co-formation of the thin and thick disks. One part of the evidence was that there is a significant population of old (chemically defined) thin disk stars in the Solar neighbourhood. The thick disk also includes stars that are older than 10 Gyr (see figure 1.2, Mackereth et al. 2019), thus some of the stars in the different disks formed at the same time. Furthermore it is shown by the presence of a peak in the pericenter distribution at $r_{\rm per} \sim 7$ kpc with contributions from both thin and thick disks. Their results disfavor a sequential formation scenario.

1.2 Galaxies in the early Universe

Galaxy shapes and kinematics are necessarily affected by processes whose effects vary with time and across galaxy masses. These include the accretion of cosmic gas, star formation, gas-rich and gas-poor galaxy mergers and interactions, feedback from intense star formation, super massive black holes, and gas outflows and gas recycling (Pillepich et al. 2019). Observing the Milky Way's past is impossible, however with the use of extragalactic observations we can get an insight of the characteristic of the Milky Way in the early universe. Disk galaxies are observed to follow general trends (Courteau et al. 2007). Properties like the gas fraction, velocity dispersion and SFR have been shown to be redshift dependent (see Saintonge et al. 2013; Wisnioski et al. 2015; van Dokkum et al. 2013), and thus will give us clues about the evolution of galaxies.

As discussed above, properties of galaxies follow several fundamental relations, which provide

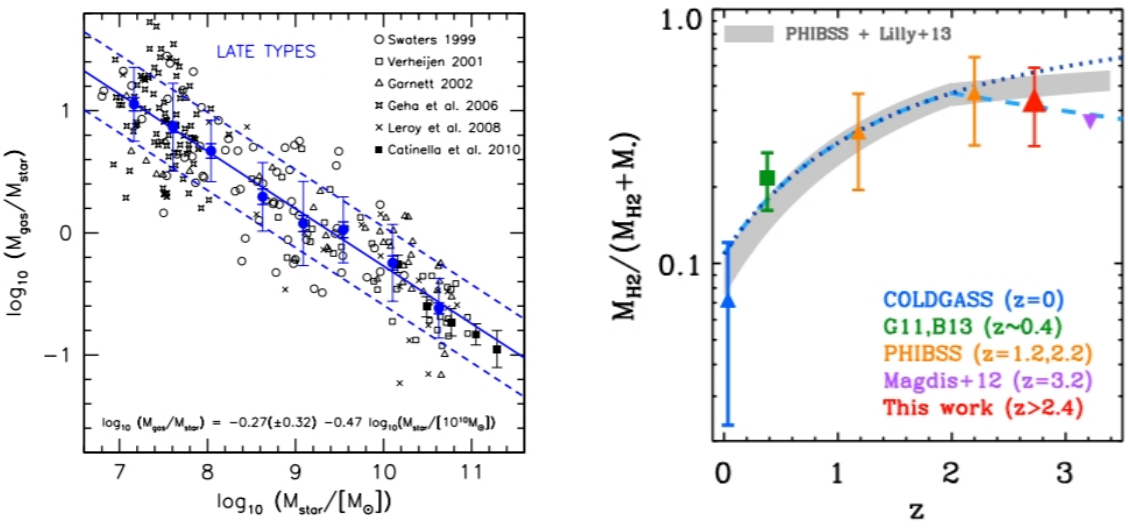

(a) (b)

Figure 1.4: Gas fraction as a function of stellar mass relation for late-type galaxies (a) and gas fraction redshift relation (b). The left figure is by Dutton et al. (2011), the gas is the cold atomic and molecular gas, including Helium. The right figure is by Saintonge et al. (2013), showing the relation for main-sequence galaxies. The different colours relate to different datasets corresponding to a redshift range.

important clues about the processes that influenced their formation and evolution. Late-type disk galaxies generally have gas fractions that increase with decreasing stellar mass or luminosity (e.g. Dutton et al. 2011). Figure 1.4a shows the relation between gas-to-stellar mass ratio and stellar mass for late-type galaxies from Dutton et al. (2011). For stellar masses above 10^{10} $M_\odot$ the mean ratio between molecular hydrogen and stellar mass is 8%, while for a stellar mass M_{star} = 10^9 $M_\odot$, the cold gas fraction is 61%. The gas fraction hence decreases with stellar mass. We know that in the past, the Milky Way was less massive and thus had a higher gas fraction. Saintonge et al. (2013) studied the gas fraction of main-sequence galaxies in relation to their redshift, shown in figure 1.4b. Galaxies in the early universe seemingly have higher gas fraction, we can thus expect that the earlier epochs of the Milky Way have very different gas fractions and stellar masses than what we observe in the current epoch.

Figure 1.5 shows the average velocity dispersions of the interstellar medium (ISM) for disk galaxies only, taken from IFS surveys with good spatial and spectral resolution by Wisnioski et al. (2015). This shows us that high redshift disks are more turbulent, with a velocity dispersion of 80 km/s at z $\geq$ 3 that decays down to 30 km/s at z = 0. This is due to the influence of a more active and gas-rich environment on the velocity dispersion. The gray band in the figure is described by

$$\sigma_z = V_{\rm rot}\ f_{\rm gas}(z)\ Q_{\rm crit}/a, \tag{1.2}$$

where $f_{\rm gas}(z)$ is the molecular gas fraction of the total mass of a galaxy as a function of the redshift, $Q_{\rm crit} = 1$ and $a = \sqrt{2}$ for a $\log(M_\star) = 10.5$ disk with constant rotational velocity (for a more detailed description of the predicted evolution, see Wisnioski et al. 2015).

The observed dispersions and predicted evolution are in agreement, indicating that the evolution of measured velocity dispersions can be described by the evolution of the gas fraction. The gas fraction in the predicted evolution depends on depletion time and the specific star formation rate, so these will be key properties in explaining the evolution of the velocity dispersion of the ISM in a disk galaxy.

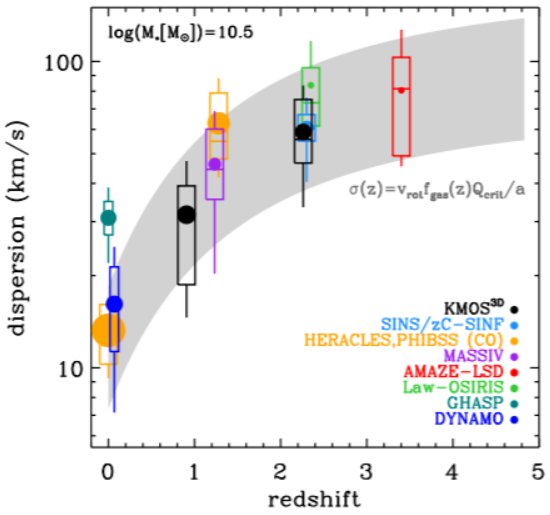

Figure 1.5: The galaxy velocity dispersion measurements from the literature at $z = 0 - 4$ from molecular and ionized gas emission. The gray band is described by equation 1.2 (Wisnioski et al. 2015).

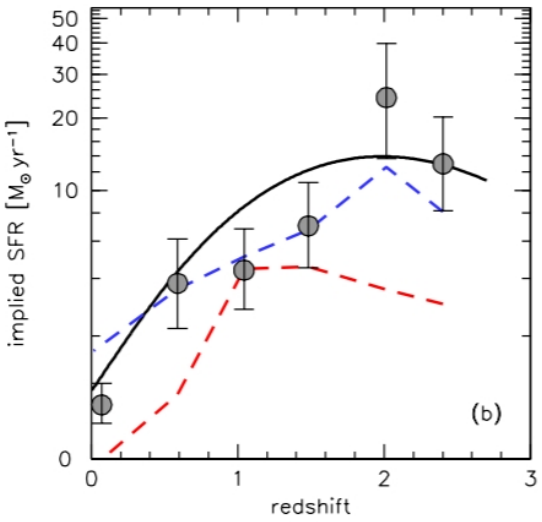

Figure 1.6: Implied evolution of the SFR. Data points are the mean measured star formation rates of progenitors of current day Milky Way-mass galaxies in each redshift bin by van Dokkum et al. (2013)

1.2.1 Star formation rates in Milky Way progenitors

As shown in figure 1.6, the star formation rate also follows a relation with redshift. The implied star formation rate as calculated by van Dokkum et al. (2013) is plotted against the redshift of Milky Way progenitors. The blue line shows this relation for SFR outside of a radius of 2 kpc and the red line shows this for inside 2 kpc. The black line is fitted using the theoretical relation described in van Dokkum et al. (2013) as

$$\log(1 + \mathrm{SFR}) = 0.26 + 0.92z - 0.23z^2 \tag{1.3}$$

The points are derived from the 3D-HST v2.1 catalogs (Skelton et al. 2014). They linked progenitor and descendant galaxies by requiring that they have the same co-moving number density, resulting in that galaxies are ranked according to their stellar mass and used galaxies at high redshift that have the same rank order as the Milky Way has at z = 0. The implied star formation rate declines abruptly after z $\sim$ 1. By z = 0 we are left with slowly star forming disks, SFR $\sim 1\ M_\odot\ \mathrm{yr}^{-1}$, as is shown in figure 1.6. The points are consistent with the theoretical model indicated by solid black line. In this project we will use this data to constrain which cosmic epoch our numerical simulations correspond to and create an understanding of the evolution of the Milky Way.

1.3 This work

To explain the observed increase in vertical velocity dispersion with age of stellar populations many often focus on secular heating (e.g. Bird et al. 2013; Aumer et al. 2016a; Grand et al. 2016). We know that stars in our galaxy follow the age-velocity dispersion relation (Aumer & Binney 2009), which can be explained partially by secular heating, but parts seems to be missing. Observations and theory indicate that the interstellar medium is highly turbulent in gas-rich galaxies, so *what role did the ISM turbulence have on the disk heating of stars?* And *are we able to explain the disk evolution and heating of the Milky Way with turbulent heating?* To answer these questions, we will try to investigate how the ISM turbulence is imprinted on

the stars that formed and its effects on thin and thick disk formation. In addition to velocity dispersion measurements, more recent studies point to the thin and thick disk having different eccentricity distributions (Li et al. 2018). The thick disk features significantly more stars on eccentric orbits than the thin disk. Next to them having clearly different distributions, Beraldo e Silva et al. (2021) used the eccentricity as evidence for an early co-formation of the thin and thick disks by showing that there exists a significant population of old thin disk stars that have ages comparable with those in the thick disk. A number of key questions on this phenomena now arise: *How was eccentricity influenced by the gas-rich past? Can we create a model on when the disks were formed using the eccentricity distribution?* We will investigate if the eccentricity values are reproducible with a purely in-situ mechanism, thus without mergers or other influences from outside the galaxy.

To conclude, in this work we explore the possibility of the thin and thick disk kinematical properties being an outcome of purely in-situ mechanisms due to the gas-rich environments in which stars form in the early Universe. In particular, we will investigate if the highly turbulent and fragmented state that we observe in high redshift galaxies can imprint thick disk properties during star formation. To address this problem, we will carry out state-of-the-art hydro+N-body simulations of entire galactic disks with gas fractions between $10-70$ percent, and compare them to observational literature data from APOGEE and Gaia. By doing so, we approximate the environmental conditions of the Milky Way's past.

1.4 Summary

Chapter 1

- The thin disk is characterized by stars on low-eccentricity orbits and thick disk has a higher fraction of stars on eccentric orbits.
- A key observable diagnostic for the formation history of the Milky Way is the age–velocity dispersion relation, whose shape is intimately related to past kinematic heating events and processes.
- There is currently no consensus on the origin of the thick disk. Different theories for the origin of thick disks invoke mechanisms such as: *gas accretion*, *mergers*, *radial migration* and *secular heating*. This project focuses on the role played by the turbulent interstellar medium, and whether it leaves a significant imprint on the stellar velocity dispersions and orbital eccentricities.
- High redshift galaxies have a higher gas fraction and velocity dispersion, thus the early Milky Way had mostly likely higher gas fraction and higher birth velocity dispersion for the stars than we experience now.

Chapter 2

Method

This work explores the possibility of the thin and thick disk properties being an outcome of purely in-situ mechanisms. To do this we adopt numerical simulations and compare them to observational data from APOGEE and Gaia. This chapter focuses on the approach for simulating galactic disks with the adaptive-mesh, hydrodynamical+N-body code RAMSES, which has been specifically designed to study the formation of structure in the Universe with high spatial resolution. The code will be discussed in section 2.1 followed by the implementation of star formation and feedback physics. In section 2.2, the initial conditions for the galaxy simulation suite are described. Finally, we outline the analysis pipeline we will be using in this project.

2.1 The RAMSES code

In this project, we use the code RAMSES (Teyssier 2002) to carry out hydrodynamical+N-body simulations of Milky Way-like galaxies with different starting gas fractions for comparison between each other and with observations. The code has been designed to study structure formation within the universe with high spatial resolution. The fluid dynamics of the baryons are calculated using a second-order unsplit Godunov method, while the collisionless dynamics of stellar and dark matter particles are evolved using the particle-mesh technique (Hockney & Eastwood 1981), with gravitational accelerations computed from the gravitational potential on the mesh.

To achieve a high spatial resolution, RAMSES makes use of Adaptive Mesh Refinement (AMR). This is a method of selectively adapting the resolution, in other words the refinement, for local regions that are of interest, such as areas with a high density. Mesh refinement is based on a pseudo-Lagrangian approach, where a cell is split if its baryonic mass (gas and stars) exceeds 8 times the baryon mass resolution. In the code, the grid is given as a hierarchical nesting of cells, where refinement happens for levels ℓ down to a new level if a higher spatial resolution is required, the other areas are left unrefined. When a cell needs refinement, it is split into 2^{dim} sibling cells that are called octs. In our 3-dimensional case, the parent cell located at level l will be split into 2^3 $(= 8)$ siblings cells. An example of AMR refinement is given in figure 2.1, which shows a snapshot of the projected gas density, with the grid structure produced by RAMSES.

The relationship between the gravitational potential and density field is given by the Poisson equation

$$\nabla^2\phi = 4\pi G\rho \tag{2.1}$$

To solve this Poisson equation, RAMSES uses the multi-grid method (Guillet & Teyssier 2011). This involves solving equation 2.1 on a level-by-level basis, beginning with the level of

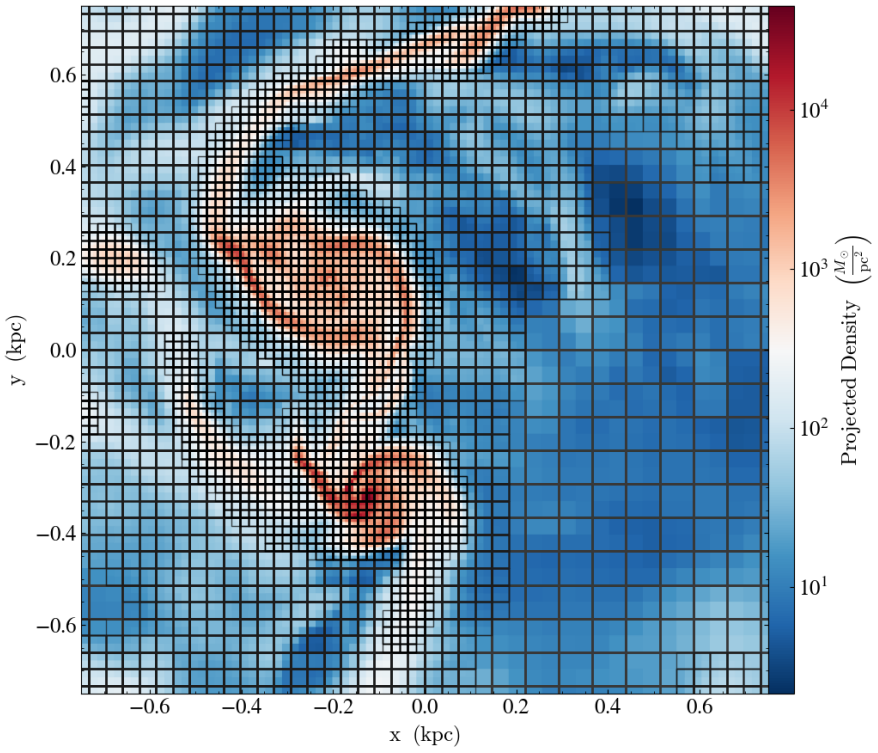

Figure 2.1: A slice-plot of simulated gas density from the `fg_50FB` galaxy at 300 Myr. This example nicely illustrates how the AMR techniques of RAMSES operates by selectively adapting the resolution in regions with a higher density. The lines indicate the grid structure in the slice of the galaxy.

highest ℓ and moving gradually towards lower levels of refinement. The potential is used to compute accelerations for both the particles and the baryon fluid.

RAMSES also includes support for hydrodynamics, which can be used to treat gas components. It solves the Euler equations (equation 2.2 - 2.4) in conservative form

$$\frac{\delta \rho}{\delta t} + \nabla \cdot (\rho \mathbf{u}) = 0, \tag{2.2}$$

$$\frac{\delta}{\delta t}\rho \mathbf{u}) + \nabla \cdot (\rho \mathbf{u} \otimes \mathbf{u}) + \nabla p = -\rho \nabla \phi, \tag{2.3}$$

$$\frac{}{\delta t}(\rho e) + \nabla \cdot [\rho \mathbf{u}(e + p/\rho)] = -\rho \mathbf{u} \cdot \nabla \phi, \tag{2.4}$$

where p is the thermal pressure, ρ is the mass density, $\mathbf{u}$ is the fluid velocity and e is the specific total energy. The gas is directly added to the grid structure, and the second order Godunov method is used to solve this set of coupled differential equations. Metals released from the star particles during the feedback (see section 2.1.1), like supernovae and winds, are treated as passive scalars and are incorporated self consistently in the cooling and heating routine.

The benefit of grid based hydrodynamics over other popular methods such as Smoothed Particle Hydrodynamics (SPH), is its ability to resolve and treat dynamical instabilities as well as mixing. The standard SPH method cannot accurately handle situations where there are steep gradients present in the density field. These situations however can be treated by grid based methods (Agertz et al. 2007). For the work presented in this project, it is essential that the turbulent instabilities resulting from the feedback processes generated by stellar populations, are accurately modelled.

2.1.1 Star formation & stellar feedback

The star formation, cooling physics and stellar feedback model adopted in the simulations is identical to the implementation used in Agertz et al. (2015), and described in detail in Agertz et al. (2013) and Agertz & Kravtsov (2015). Star formation is modelled using the so-called Schmidt law, which relates the star formation rate density , $\dot{\rho}_\star$, to the gas density, ρ_g, as

$$\dot{\rho}_\star = \frac{\rho_g}{t_{\rm SF}} \text{ for } \rho_g > \rho_{\rm th}, \tag{2.5}$$

where the star formation threshold on the gas density is $\rho_{\rm th} = 300$ m$_{\rm H}$ cm^{-3}, the typical average density of GMCs in the Milky Way. Furthermore, $t_{\rm SF}$ is the typical time scale for galaxies to convert their gas into stars, also denoted as the star formation timescale. The stars will be grouped together as star particles in the simulations, representing a single stellar population with an internal initial mass function (IMF), notably, the canonical Chabrier IMF (Chabrier 2003). The initial mass of a star particle is $m = 10^3\ M_\odot$, this mass changes as stars shed material through stellar winds and supernovae. A discrete Poisson distribution is used to determine the number of star particles which form during each star formation event.

In this project we assume $t_{\rm SF}$ to be

$$t_{\rm SF} = \frac{t_{\rm ff}}{\epsilon_{\rm ff}} = \frac{1}{\epsilon_{\rm ff}} \sqrt{\frac{3\pi}{32 G \rho_g}}, \tag{2.6}$$

$t_{\rm ff}$ is the local free-fall time, and $\epsilon_{\rm ff}$ describes the fraction of gas that forms stars every free-fall time, thus the star formation efficiency per free-fall time. Another criterion for star formation is set in terms of the gas temperature, star formation will only occurs in cells containing cool gas (T $<$ 100 K). No other criteria on the environmental properties are enforced on the star formation.

The degree to which feedback affects the evolving galaxy in numerical simulations can depend on the adopted value of the star formation efficiency (Agertz & Kravtsov 2015). This parameter likely depends on the scale and environment of the region, and the physical processes that control how efficiently gas gets turned into stars are not yet fully understood. Nevertheless, empirical relations exist, which indicate $\epsilon_{\rm ff} = 0.001 - 0.3$ for individual star-forming regions in the Milky Way (Lee et al. 2016). It has been shown that for feedback to sufficiently regulate star formation, a local star formation efficiency per free fall $\epsilon_{\rm ff} = 10\%$ produces results that agree well with observed properties of the ISM (Grisdale et al. 2017, 2018, 2019)

The feedback is implemented using the methods described in Agertz et al. (2013) and Agertz & Kravtsov (2015). Several processes contribute to the stellar feedback, as stars inject energy, momentum, mass, and heavy elements overtime via supernova type II (SNII) and supernova type Ia (SNIa) explosions, stellar winds, and radiation pressure into the surrounding interstellar medium. The spatial resolution is not always high enough to resolve the early energy driven evolution of SN explosions. To account for the effect of SN feedback, we adopt the model suggested by Kim & Ostriker (2015). They demonstrated that in order to capture the momentum injection from individual supernovae, the cooling radius must be captured by at least three grid cells to avoid numerical overcooling (see also Martizzi et al. 2015). In this work we therefore adopt three grid cells per cooling radius as a minimum requirement for supernovae to be considered as resolved.

2.2 Simulation suite of galaxies

The initial composition of the galaxies is created by distributing the dark matter and stars as particles and gas initialized on the adaptive mesh. The simulations in this project uses $N = 10^6$ particles. Nonetheless, the galaxy first needs to “relax” before it resembles a disk galaxy. With

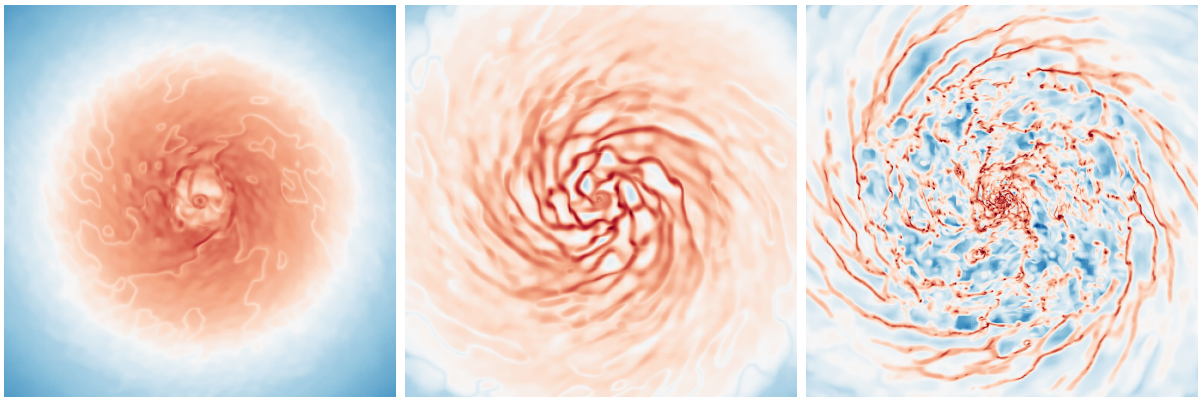

(a) (b) (c)

Figure 2.2: The projected gas density field at, from left to right, $t \approx 30, 100$ and 150 Myr for the simulation with 30% gas fraction (f_g). The colour scheme indicates the density of the gas, ranging from diffuse (blue) to dense (red/dark red). Panel (a) illustrates the "relaxation phase", where the simulations is run at low spatial resolution without stellar feedback (see main text). Panel (b) shows the development of spiral structure, and is the point in time where we decide to increase the spatial resolution and activate stellar feedback. Finally, panel (c) shows the simulation after this 'relaxation phase', at a higher resolution and with stellar feedback.

"relaxing" we mean that we first run the simulation with a low resolution and without feedback. This allows for a slightly less violent transition from the artificial and smooth initial conditions (ICs) to a structured disk. Figure 2.2a shows the beginning of the simulation, in the "relaxation" phase with a low resolution. We then follow the simulation and when we see strong a presence of a spiral disk (figure 2.2b), we turn on the feedback and go to a higher resolution (figure 2.2c), this is purely done by eye and is thus not a precise technique. This "relaxing" happens on a dynamical time scale, which is roughly one rotation period of the galaxy. For higher gas fractions, we expect the "relaxation" time to be shorter as they undergo clumping much earlier. After this, the simulations are run for an extra $t \sim 250$ Myr, and analysis on the simulations can be done.

2.2.1 Galactic initial conditions

The simulations have galactic parameters chosen to mimic a Milky Way-sized galaxy at different redshifts. The initial conditions were derived from the isolated disk galaxy in the AGORA project (Kim et al. 2014, 2016), set up to approximate a Milky Way-like galaxy following the methods described in Hernquist (1993) and Springel (2000). All the variables required to derive the structural setup for the galaxies in the simulations are shown in table 2.1. For the dark matter halo the Navarro-Frenk-White profile (Navarro et al. 1996) is adopted with a concentration parameter $c = 10$. The dark matter spin parameter λ is set to a value of $\lambda = 0.05$ (Bullock et al. 2001). The virial circular velocity $v_{200} = 150$ km/s and halo virial mass $M_{200} = 1.1 \times 10^{12}$ $M_\odot$ within a virial radius of $R_{200} = 205$ kpc. The initial stellar and gaseous components follow exponential surface density profiles with scale lengths $r_d = 3.43$ kpc and scale heights $z_d = 0.1 r_d$. Furthemore, the bulge-to-disk mass ratio is 0.125 and the bulge mass profile is that of Hernquist (1990) with scale-length $0.1 r_d$. The halo and stellar disk are represented by 10^6 particles each, and the bulge consists of 10^5 particles.

2.2.2 Simulation runs

For this project we use six different simulations with different gas fractions. The initial conditions given in table 2.1 were chosen in order to simulate a galaxy with a Milky Way-like mass at

	fg10	fg15	fg20	fg30	fg50	fg70
Stellar disk mass, $M_{d,\star}$ [10^8 $M_\odot$]	386.9	365.4	343.9	300.9	214.9	128.9
Stellar bulge mass, M_b [10^8 $M_\odot$]	43.0					
Dark matter halo mass, M_h [10^{10} $M_\odot$]	125.5					
Gas fraction, f_g	0.1	0.15	0.2	0.3	0.5	0.7
Dark matter concentration factor, c	10					
Gas metallicity, $[Z_\odot]$	1.0					
Scale height disk, z_d [kpc]	0.34					
Scale radius disk, r_d [kpc]	3.43					
Scale radius bulge, r_b [kpc]	0.3432					

Table 2.1: Initial conditions used for the simulations with the different gas fractions.

different stages of its evolution, as demonstrated in chapter 3. The gas fraction will act as a proxy for the evolution, as discussed in section 1.2. We stated that a lower stellar mass relates to a higher gas fraction for a galaxy and that high redshift galaxies are observed to have higher gas fractions in general. To get a good idea on the influence of the gas fraction on the disk evolution, we will use simulations with gas fractions of 10%, 20%, 30%, 50% and 70% for most of our analyses. We eventually will also be using a simulation with a gas fraction of 15%, which will only be used when we are trying create a fit using different eccentricities of the gas fractions and constrain the ISM during disk formation (section 3.4.3). The simulations with a gas fraction of 10% and 50% have been run by Ejdetjärn (2019), the other simulations have been carried out specifically for this project. The computational resources came from the Aurora servers at LUNARC[1], a centre for supercomputing at Lund University.

The simulation box used in all the different simulations is a cube with sides of 600 kpc length with adaptive mesh refinement allowing for a minimum cell size of 9 pc. As discussed, the AMR scheme splits cells into 8 new cells, these cells will each have a mass of $m_{\text{refine}} = 4014$ $M_\odot$, when their sum of stellar and gas mass exceeds 8 $\times m_{\text{refine}}$. The boundary conditions of the simulation box allow for the outflow of material, the large box and boundary conditions are chosen to mimic the environment of an isolated galaxy.

2.3 Data analysis

From the output data of the simulations run with the RAMSES code, we can extract all the different properties of the gas and stars present in the simulations. To do this we use the analysis tool `yt` project version 3.6.0[2] (Turk et al. 2011). The yt project environment also provides derived fields along with a set of plotting options. In this project `yt` project is used mainly to extract the properties of the stars and connected to self-written pipelines in python for analysing and plotting the data.

[1] `https://www.lunarc.lu.se`
[2] `https://yt-project.org`

2.3.1 Velocity dispersion

In this project, we investigate the formation of the thin and thick disk in relation to in-situ mechanism. As discussed in section 1.1.1, the velocity dispersion is one of the properties that differentiates the thick and thin disks. Therefore, the velocity dispersion will be one of the main properties we will be using to compare to observations. The velocity dispersion of the different simulations and at different times, will be calculate using

$$\sigma = \sqrt{\frac{\sum_{i=0}^{N}(v_i - \bar{v})^2}{N}}, \tag{2.7}$$

Hence, N is the sample size, v_i the velocity of an individual star and $\bar{v}$ the average velocity of the group. The velocity dispersion is the statistical dispersion of velocities about the mean velocity for a group of stars. We want to investigate how σ depends on the position in the galaxy and how it evolves. Therefore, we used two different ways of dividing the sample sizes, on radius and on the age of the stars. To get the most data points, we tried to make the bins as small as possible, while still being able to calculate the statistical dispersion. We consider radial bins for size $\Delta_R = 1.2$ Kpc. For the age bins we consider $\Delta_{\text{age}} = 10$ Myr for the `fg10` simulations, for the others we consider $\Delta_{\text{age}} = 25$ Myr.

2.3.2 Radial evolution of the stars

Another property used to separate the thin and thick disk is the eccentricity of the stars as discussed in section 1.1.2. To investigate the eccentricity distribution of the stars in our different simulations, we need to obtain the galactocentric radius evolution of the stars. To get the radii through time, we extract the IDs and radii of the stars from the simulation. This will give us a table where we can see all the stars and their location over time, this process is shown in figure 2.3. Showing first the separate tables we can extract from the different times using `yt` project. Then these tables are separately ordered on their ID list, so that the first row of each table corresponds to the same star. These tables can then be combined together to form one table including all the stars and their radial evolution through all the different time steps.

Using this table we can calculate the eccentricity using equation 1.1, using the minimum and maximum radius of our table for each star. To make sure the stars had enough time to be heated, we will only include stars that were born in the first time step after feedback has been implemented, which is around 100 Myr (see figure 3.2 in section 3.1.1). This will ensure that all the stars went through ~ 1.5 orbits before we calculate the eccentricity.

2.4 Summary

Chapter 2

- We evolve a set of disk galaxies, using the N-body+hydrodynamical code RAMSES. The simulations consider galaxy physics such as cooling, star formation and feedback.
- The initial conditions represent a Milky Way-like galaxy, but at different gas-fractions in order to approximate the galactic conditions at different stages.
- The outputs are analysed with a self-written Python code, both for plotting and deriving quantities. Extracting the outputs and the projection plots are done with the analysis tool `yt` project version 3.6.0

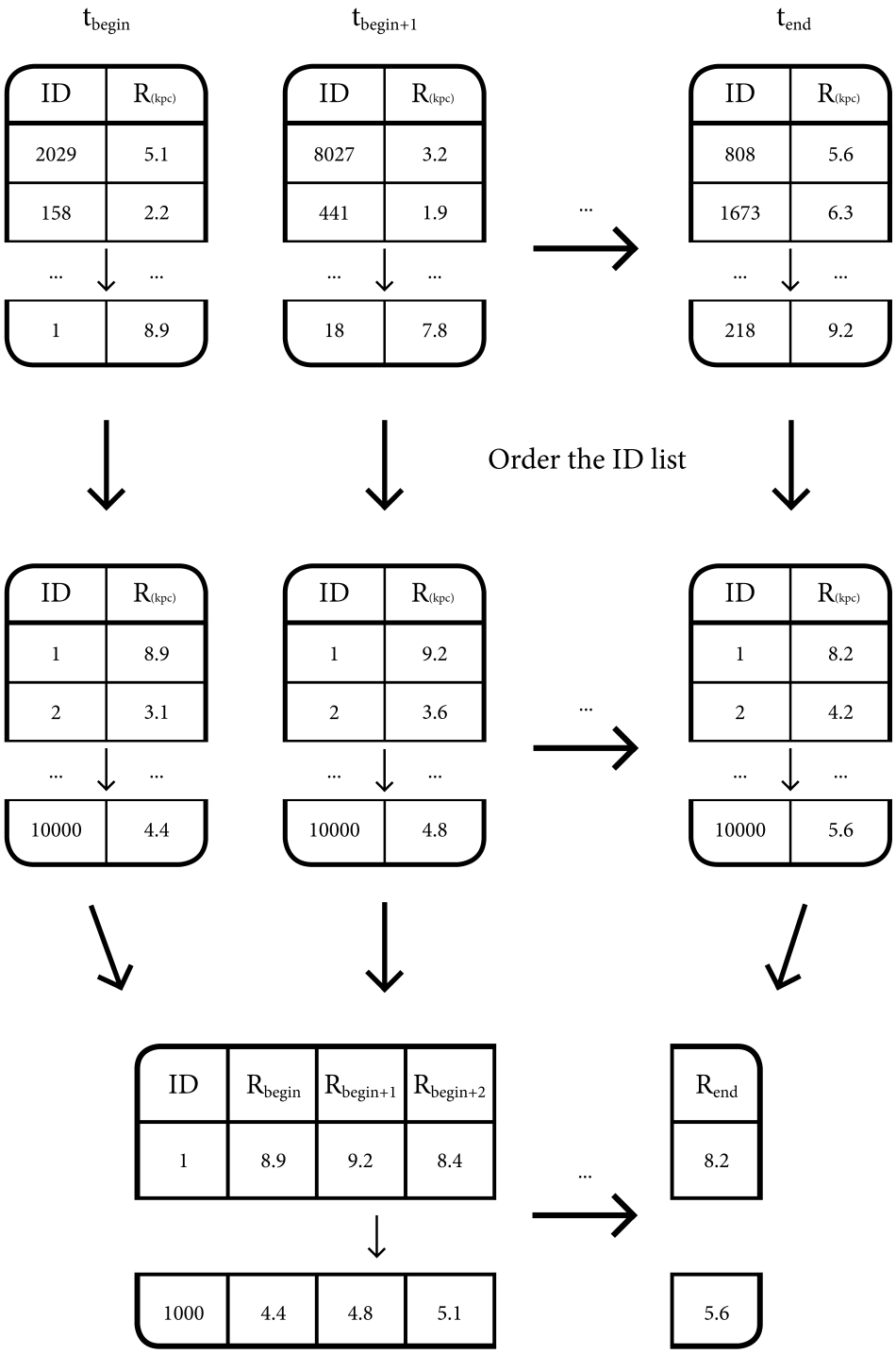

Figure 2.3: Infographic showing the process of getting the radii at each time step for each star. First we extract separate tables from the different time steps using `yt` project. These tables include the ID of a star and its galactocentric radius at that moment in time. These tables will then be ordered on their ID list, so that the first row of each table corresponds to the same star. These tables can then be combined together to form one table.

Chapter 3

Results

This chapter presents the analysis of the simulated galaxies with the different galactic initial conditions as described in Table 2.1. In chapter 1 we showed that the gas fraction of a galaxy increases with a decreasing stellar mass and that galaxies will be more gas-rich at higher redshifts (Dutton et al. 2011; Pillepich et al. 2019). To investigate the conditions of the stars in earlier epochs of the Milky Way, we modify the gas fractions of simulated galaxies of the same size and total mass. Changing the gas fraction is a useful and efficient way to understand the impact of the gas-rich early stages of galaxy evolution. We note that a more complete treatment would include the full cosmological environment. However, our strategy allows us to carry out a controlled study, without e.g. the influence of mergers.

We start with an analysis of general galactic properties, including a visual inspection of the gas density field, star formation history, and evolution of the gas fraction of the disk. We do so in order to illustrate how the simulations correspond to different epochs in a Milky Way-mass galaxy's past. Secondly, we present one of the key results of this project, the level of vertical stellar heating, and compare our results to observational data from Gaia and APOGEE. Next, we quantify how the different gas fractions affect the orbital properties of the stars and compare this to observational data. Finally, we discuss the implication of our results for the Milky Way's formation history.

3.1 General properties of simulated galaxies

Figure 3.1 shows the gas and stellar density projections of each simulated galaxy at 300 Myr with initial gas fractions of 10%, 20%, 30%, 50%, and 70% gas (see Table 2.1). It is clear from the gas density projections that flocculent spiral structures are present in all the galaxies, although less so in the highest gas fraction cases. Furthermore, we see the presence of massive clumps, in particular in the `fg30`, `fg50` and `fg70` simulations, which is compatible with observations of gas-rich high redshift galaxies (see e.g. Elmegreen et al. 2009; Dessauges-Zavadsky et al. 2019). There is a clear relationship between the prominence of galactic outflows and increasing gas fraction, which is evident in the edge-on view of the gas density projection in figure 3.1. From this, we can see that there is a more irregular and turbulent Interstellar Medium (ISM) at the higher gas fractions regimes that will impact the birth properties of the stars.

3.1.1 Gas fraction & star formation histories

In this study, the gas fraction is the only modified property between the different simulated galaxies. Figure 3.2 shows how the mass fraction of gas evolves over time. To compute the gas fraction, we consider only the cold/warm ISM ($T < 10^4$ K). Indicated in gray is the relaxation period described in section 2.2. As is evident in the figure, this relaxation period was chosen by eye and therefore not the same for all the simulations.

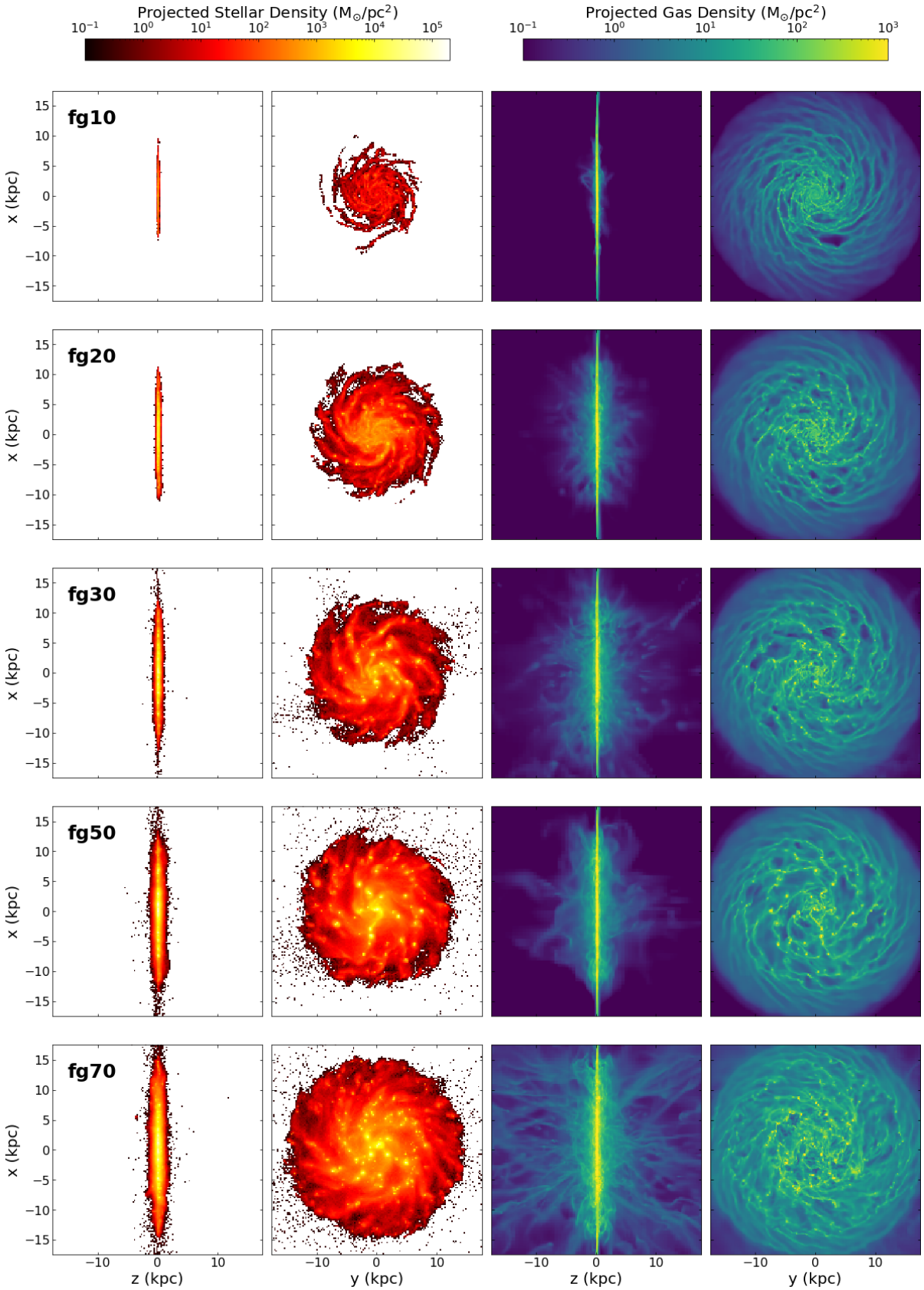

Figure 3.1: Stellar (left) and gas (right) density projections of the simulated galaxies at 300 Myr. The gas fraction increases from top to bottom from 10% to 70%. The gas density projections show the presence of flocculent spiral structure in all galaxies. In the higher gas fraction regimes, there is a clear presence of massive clumps and more irregular and turbulent ISM.

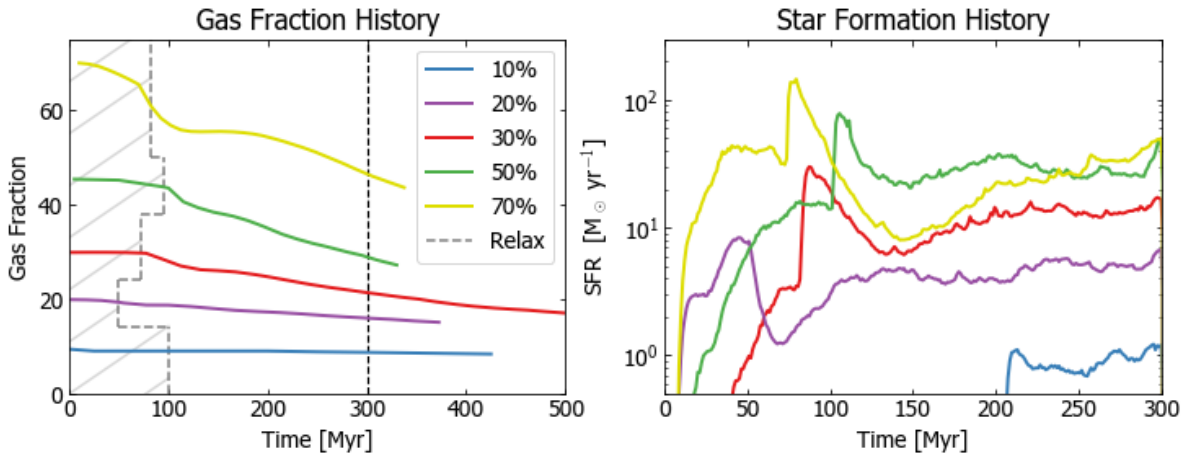

Figure 3.2: The gas fraction (left) and star formation rate (right) over time for the different simulations. The relaxation phase is shaded gray in the left panel and the vertical dashed black line shows the time of analysis.

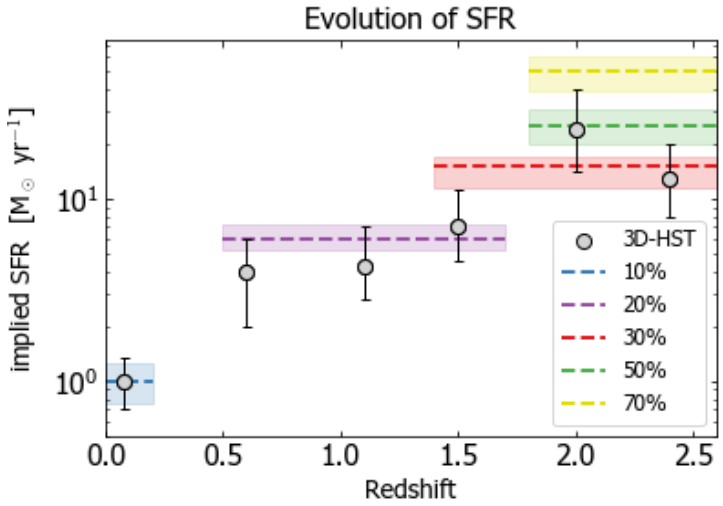

Figure 3.3: Implied evolution of the star formation rate of Milky Way-mass progenitors (gray points) with the star formation rate of our simulations at ± 300 Myr shown as bands. The vertical thickness of the bands represents the standard deviation from the 150 Myr to 300 Myr. The data points are the mean measured star formation rates of the galaxies in each redshift bin, from the 3D-HST v2.1 catalogs (van Dokkum et al. 2013; Skelton et al. 2014)

Star formation and outflows lower the gas fraction in all simulations, which makes the gas mass-loss rates higher for higher initial gas fractions. To make meaningful comparisons between the simulations, we carry out all analyses at t=300 Myr (∼ 1.5 orbits), indicated in the left panel of figure 3.2 with a vertical black dashed line, and only include the stars formed after the relaxation phase. From this figure, we can see that the gas-rich galaxies deplete their gas reservoir faster than the gas-poor galaxies. For example the `fg70` simulation evolves from $f_g \sim$ 70% to ∼ 50% gas, whereas `fg10` will also deplete gas but stays around 10% gas.

In the right panel of figure 3.2, the star formation rate history of the galaxies are shown. The overall SFR mainly increases with increasing gas fraction. In general, We find that the simulations with a lower gas fraction have a lower SFR, e.g. at 300 Myr we have `fg10` with an SFR of ∼ 1 $M_\odot$ yr^{-1} and `fg20` of ∼ 6 $M_\odot$ yr^{-1}, compared to the higher gas fractions, e.g. ∼ 15 $M_\odot$ yr^{-1} for `fg30`, ∼ 30 $M_\odot$ yr^{-1} for `fg50` and ∼ 50 $M_\odot$ yr^{-1} for `fg70`. This can be the

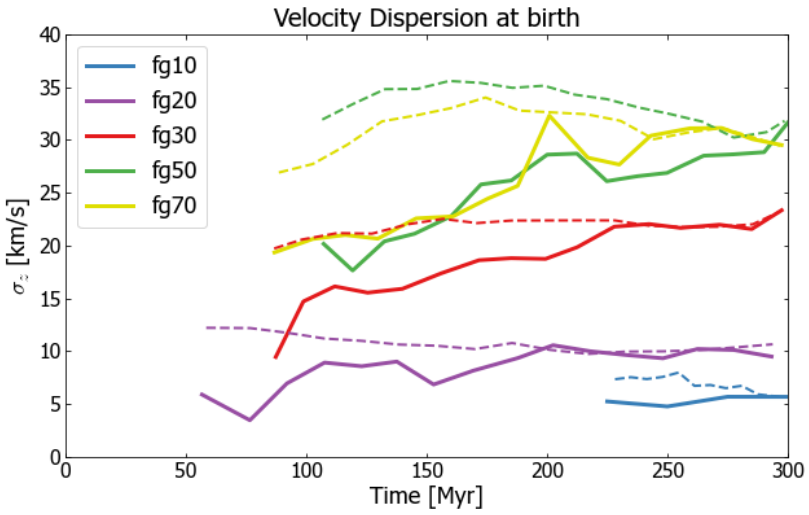

Figure 3.4: Solid lines: The vertical velocity dispersion at birth as a function of simulation time. Stars born around 300 Myr have a higher σ_z at birth than stars born in the beginning of the simulation, due to the gradual buildup of turbulence in the ISM. Dashed lines: The measured vertical velocity dispersion of stars born at the times indicated by the x-axis, but measured at 300 Myr, e.g. stars born at 50 Myr in an environment with $f_g = 20\%$ went from ~ 5 km/s at birth (solid line) to ~ 13 km/s at 300 Myr.

effect of two things. One reason could be that less gas will be available above the star formation density threshold. The other reason could be that the gas is denser in high gas fraction galaxies (see figure 3.1), meaning that there will be a shorter depletion time and thus a higher SFR. Furthermore, in figure 3.1 we see that the higher gas fraction simulations have more clumps and thus point to both of these possibilities being present in our simulations. Lastly, we note that the `fg10` simulation only forms stars after 200 Myr, in contrast to the other runs that already form stars during their relaxation phase. This is due to the time required to develop dense GMCs in which stars form, which takes longer in a lower gas fraction regime.

We compare the simulated SFRs to the observationally inferred star formation histories by van Dokkum et al. (2013) (see section 1.2.1). This allows us to estimate the cosmic epoch that each simulation corresponds to. The data points shown in figure 3.3 indicate the mean observed star formation rates of Milky Way progenitors as a function of redshift using the 3D-HST[1] v2.1 catalogs (Skelton et al. 2014). The coloured bands show the SFRs measured at 300 Myr[2] from the simulated galaxies. We have placed them, by eye, at a redshift range where there is significant overlap with observations. We note that this is a crude and approximate approach which should only be considered as indicative. As can be seen in the figure, the $f_g = 10\%$ simulation overlaps with galaxies at $z \sim 0$, $f_g = 20\%$ corresponds to $z \sim 0.5 - 1.7$ and so forth. All simulations can be matched to observations in this approximate way, with the possible exception of the 70% gas fraction galaxy. However, it is compatible with the $z \sim 2$ data at a 2σ level, and we therefore consider it as a viable model for starbursting, high redshift Milky Way progenitor.

3.2 Vertical heating and the "turbulence barrier"

We next turn to an analysis of the vertical kinematics of the stars in the different gas fraction environments. Figure 3.4 shows the vertical velocity dispersion of the stars at birth for the

[1] A spectroscopic Galaxy Evolution Survey with the Hubble Space Telescope
[2] The error margins are done by eye, looking at the deviation of SFR between 250 and 300 Myr.

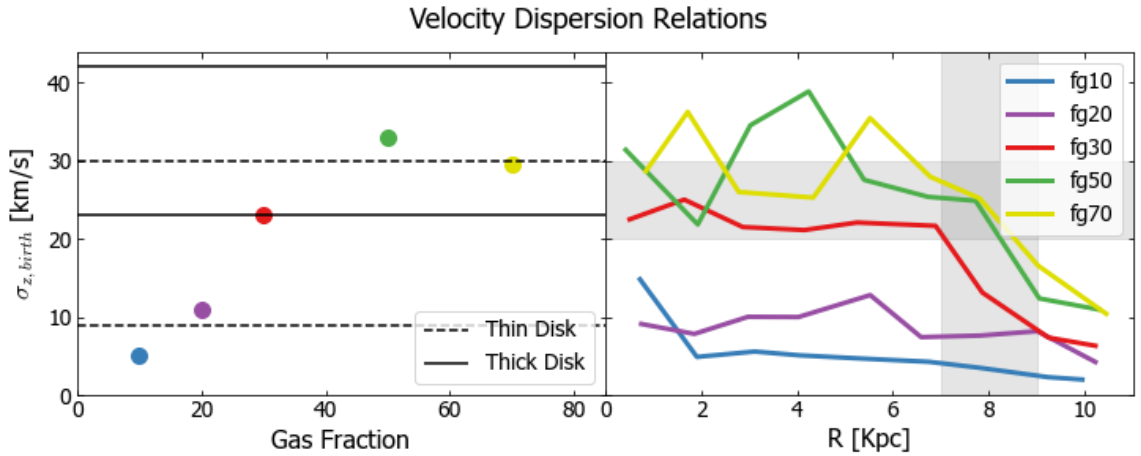

Figure 3.5: Vertical velocity dispersion as a function of galactic gas fraction at 300 Myr (left panel) and radial dependence velocity dispersions relation for stars that are 50 Myr and younger (right panel). The vertical lines in the left panel indicate the upper and lower bounds for the velocity dispersion in the chemical thin and thick disk. In the right panel, the vertical gray shaded area indicates the location of the Milky Way Solar neighbourhood (MW Snhb) and the horizontal area indicates the velocity dispersion values we observe in the MW Snhb (Mackereth et al. 2019)

simulations. It is expected that stars born in higher gas fraction regimes will have a higher σ_z at birth, because stars will form out of the turbulent ISM and the levels of turbulence is higher in the gas-rich high redshift galaxies (see section 1.2). In addition, we would also expect that scattering by perturbation in the disk due to GMCs and spiral arms (see section 1.1.1) will lead to an increasing vertical velocity dispersion for older stars (Aumer et al. 2016a). As such, $\sigma_{\mathrm{z,birth}}$ should be considered as a lower limit. Furthermore, given the greater prevalence of massive GMCs in the higher gas fraction models, it is expected that stars will be more vertically heated over time in these runs. In the same figure, the dashed line indicates to which σ_z the stars are heated at 300 Myr. It demonstrates that the heating of stars over time is important, but that the environment the stars were born at, $\sigma_{\mathrm{z,birth}}$, should not be neglected.

The oldest stars in each galaxy are heated to the same σ_z level as newly born stars in the simulations. This indicates that the level of turbulent heating is not fully developed at the early stages of our simulations, therefore we will be using $\sigma_{\mathrm{z,birth}}$ at 300 Myr in our subsequent analyses.

The left panel of figure 3.5 shows how the gas fraction relates to $\sigma_{\mathrm{z,birth}}$ for the stars born in different gas fraction regimes, which gives us a better understanding of the importance of the environment the stars are born at. The $\sigma_{\mathrm{z,birth}}$ is determined at 300 Myr. The vertical lines in the figures indicate the lower and upper bounds in the Milky Way thin and thick disk as analysed by Mackereth et al. (2019) between the ages of 1 and 10 Gyr (see section 1.1.1). The simulation with gas fraction 30% is located at the transition between the thin and thick disk formation, this indicates that a thin disk, with $\sigma_z < 22$ km/s, is impossible to form for $f_g \geq 30\%$. The level of ISM turbulence is simply too high since the stars will only be heated further over time. Therefore $f_g = 30\%$ simulation is acting as a *"barrier"* against the formation of a kinematically cold disk. Another interesting aspect of figure 3.5 is the 50% and 70% gas fraction points. The vertical velocity dispersion relation seemingly increases with the gas fraction till it hits the 50% and 70% gas fractions points. This may indicate a maximum level of ISM turbulence produced via gravitational instabilities and stellar feedback in our simulations as they also have a similar SFR.

The right panel in figure 3.5 shows the radial dependence of the vertical velocity dispersion relation for the stars with a maximum age of 50 Myr in the different runs. The vertical gray

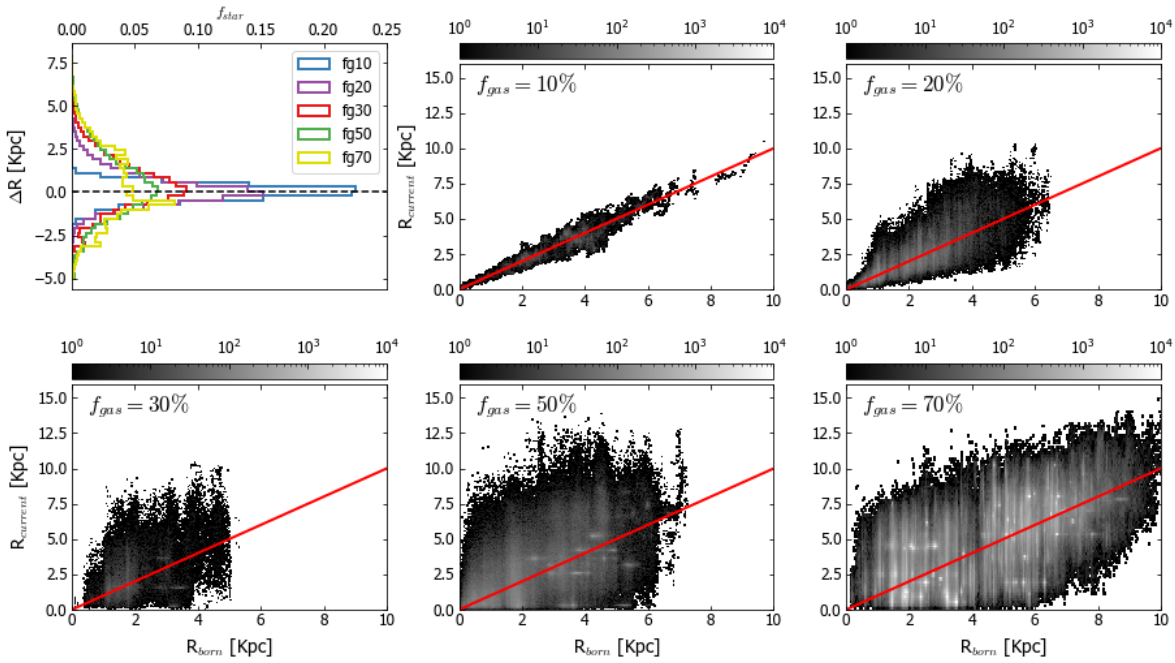

Figure 3.6: Visualisation of the changes in galactocentric radius of the stars between their birth and 300 Myr. The upper left panel shows a distribution of the movement of the stars with negative values meaning that it moved towards the center of the galaxy. In the other panels the birth radius is plotted against the current radius for the stars in the different runs.

shaded area indicates the location of the Milky Way Solar neighbourhood. In this figure, we can see that the velocity dispersion also depends on the galactocentric radius. Furthermore, we find that all the different runs give values that are in line with observations done in the Solar neighbourhood (< 30 km/s, Nordström et al. 2004; Mackereth et al. 2019), even for the higher gas fractions. However the initial conditions are idealized, and the extent of the gas disk may not be fully captured. The velocity dispersion at a given radial position in the galaxy is influenced not only by heating processes at the position but also by migration. Stars with a different velocity dispersion can migrate, and increase or decrease that of a non-migrating population. Thus to get a better understanding of how the heating turbulence is imprinted on the stars that form, the next step is to investigate the orbital properties of the stars in the different ISM environments.

3.3 Orbital properties of stars

Figure 3.6 shows the current (= at 300 Myr) radius of the stars against the birth radius. The upper left panel shows the distribution of the radial movement of the stars, $\Delta R = R_{\rm curr} - R_{\rm born}$, where $R_{\rm curr}$ is the position of the star at 300 Myr and $R_{\rm born}$ is the radius of the star when the ID of the star is new to a time step. A negative value means that the star moved towards the center of the galaxy. Both blurring and churning contribute to radial movement of the stars, with some stars actually migrating to a new guiding radius and some that are simply eccentric. In section 3.3.1 we will investigate the second option further. We note that the simulations have different ranges in which stars form.

The panels of figure 3.6 show us that we measure a greater spread in ΔR, over the considered period of time, for the galaxies with a higher gas fraction. We find distinct clumps and streaks in the `fg50` and `fg70` simulation (bottom middle and right panels). In a video[3] we illustrate

[3]Video of `fg50`: `https://youtu.be/gjmF-fPspqU`

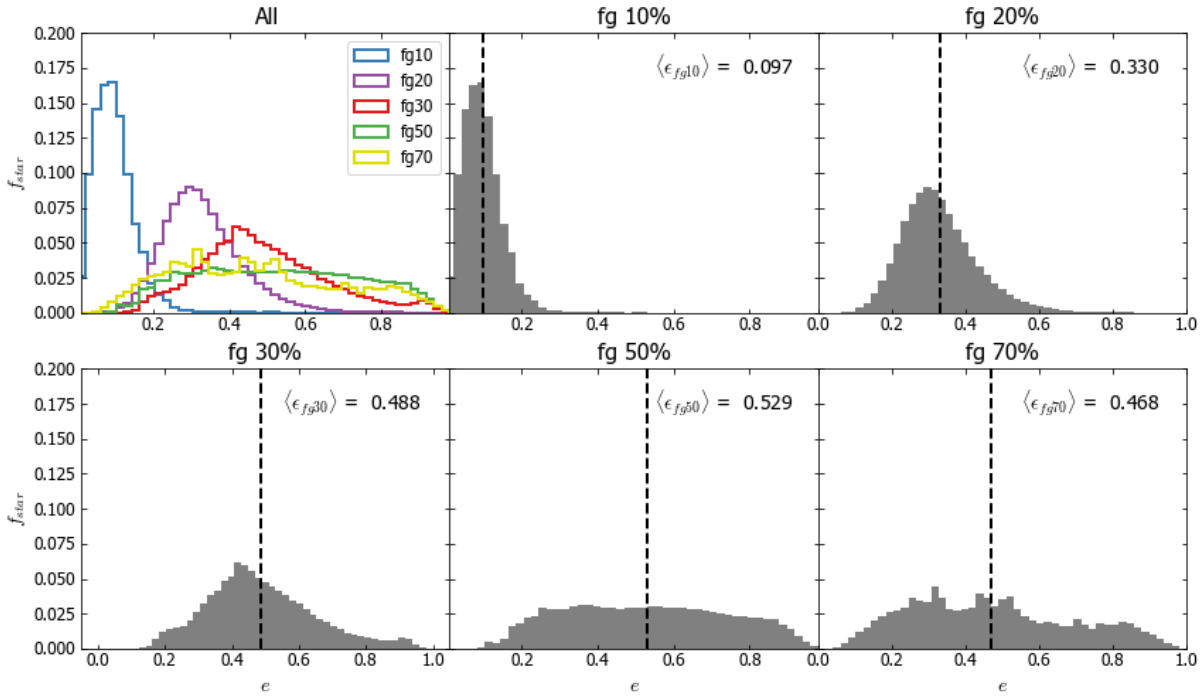

Figure 3.7: The eccentricity distribution for the different simulations. The upper left panel includes all the simulations and the other panels are the simulations separately. The horizontal dashed black line indicates the mean eccentricity, also shown in the top right corner.

the evolution of the plot for `fg50` over time. It shows the creation of the streaks and clumps. One explanation for theses streaks is that when the stars form in close proximity to eachother, they will likely migrate together and the massive star cluster loses the looser bound stars due to gravitational interaction in the disk. Another explanation for these streaks are stars with a high eccentricity. These stars will move up and down in our plot, as our simulation time is approximately 1.5 orbits.

3.3.1 Eccentricity

Figure 3.7 shows the planar eccentricity of the stars for the different simulations, calculated using the method described in section 2.3.2. As expected from figure 3.6, the lower gas fraction runs feature stars on mostly circular orbit, e.g. `fg10` has a mean eccentricity of 0.1. As the gas fraction is increased the eccentricity distribution shifts to higher values with significantly larger mean eccentricities. Simulations with $f_g \geq 30\%$ have a similar mean eccentricity of ~ 0.5, but they have very different eccentricity distributions. The distribution of $f_g = 50\%$ and 70% are significantly flatter. A reason for the similar mean and shape could be that at a gas fraction of $> 30\%$ the stars already experience a maximum amount of turbulence that leads to a higher eccentricity.

Figure 3.8 displays the eccentricity of stars at different galactocentric radii. We can see that the further the stars are from the galactic center, the more circular the orbits of the stars become. A reason for this phenomena is that at a greater distance from the galactic center there are less clumps that contribute to the heating, and thus eccentricity of the stars. The gas turbulence could be another explanation, the gas will be less turbulent and fragmented at the outskirts of the disk. Furthermore, stars closer to the galactic center will have a shorter orbital time and thus have a higher probability to get heated up.

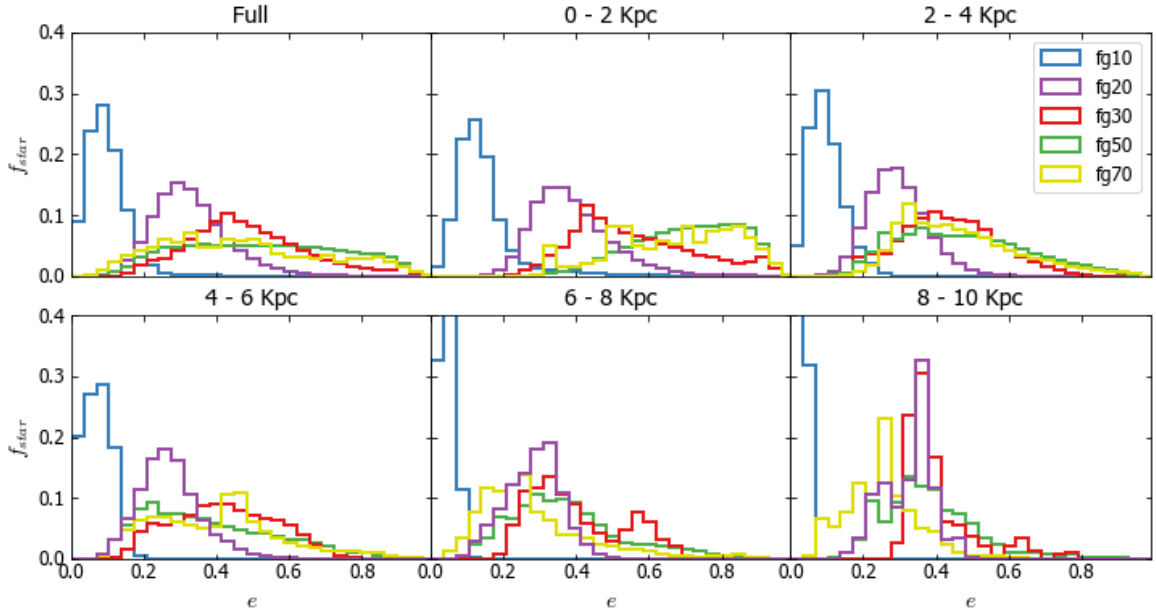

Figure 3.8: The eccentricity distribution for the different gas fraction simulations at different galactocentric radii. The stars are binned using their current (= 300 Myr) radius in the simulation.

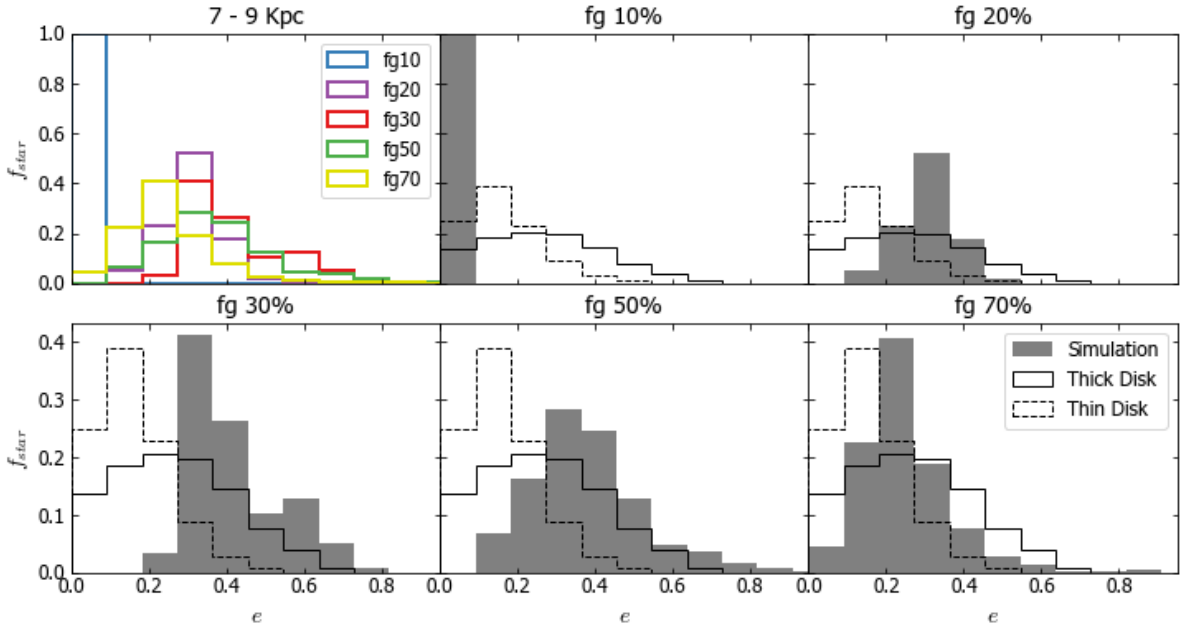

Figure 3.9: Distribution of the orbital eccentricity of the disk stars in the solar neighbourhood. The solid and dashed lines denote the thin and thick disks observations from Li et al. (2018). The eccentricity distribution from the different simulations is shown by the gray bins.

3.3.2 The Solar neighbourhood

In figure 3.9 we compare the eccentricity distributions of our simulated galaxies at different gas fractions to observations in the Milky Way Solar neighbourhood. The observational data is derived from the APOGEE data release 13 and Gaia Tycho-Gaia by Li et al. (2018). The peak value of the eccentricity distribution for thin disk stars in this data set is less than 0.2. This implies that the thin disk stars possess near-circular orbits. In contrast, the peak value of the eccentricity distribution for thick disk stars in this data set is between 0.2 and 0.3, and a significantly larger fraction of stars are on more eccentric orbits. The thin disk stars also have a smaller range of eccentricity values, between 0 and 0.55, in comparison to the thick disk stars, that have stars with an eccentricity as high as 0.75.

Comparing the eccentricities in our simulations to that of the observations, seemingly demonstrates that no single simulation can fully account for the observed distribution of eccentricities. The fact that no single simulation reproduces the entire range of eccentricity comes as no surprise since the Solar neighbourhood stars must likely have been formed in a wide range of different gas fractions. We note that the high eccentricity end of $f_{\rm g} = 30\%$, 50% and 70% matches the high eccentricity tail of the thick disk as observed by Li et al. (2018). This indicates that the high eccentricity values observed in the Milky Way can be the result of in-situ evolution. We return to this in section 3.4.3, where we will quantify the ISM needed during disk formation without mergers and influences from outside the galaxy.

3.4 Implications for the evolution of the Milky Way

Having established the impact of the gas fraction on vertical kinematics and orbital properties, we next turn to an analysis of the implications of our results for the evolution of the Milky Way. We regard this as exploratory work given the simplified assumptions we make. We start by investigating the heating of the system, in section 3.4.1 we will focus only on the turbulent preheating. In section 3.4.2 we compare our heating relations to observations by Mackereth et al. (2019) and comment on the AVR and the addition of secular heating. Next we will try to constrain the ISM during the thick and thin disk formation, thus understanding when and under which conditions the stars in the thick and thin disks are formed, using the determined eccentricity and observations from Li et al. (2018).

3.4.1 Turbulent heating of stars in different gas fraction regimes

Using our simulations, we next construct an age-birth velocity dispersion relation relevant for Milky Way-like galaxies. To do so, we map the redshift range of each simulation, as obtained in figure 3.3, to the corresponding velocity dispersion presented in the left panel of figure 3.5. The resulting relation is shown in figure 3.10, and should be considered as a *minimum* level of the stellar velocity dispersions imprinted by the gas turbulence. Also shown in the figure is a non-linear least squares fit to our results using a relation of the kind

$$\sigma_{\rm birth} \propto \exp(t). \tag{3.1}$$

This functional form is commonly considered in the literature and is good fit to data and numerical experiments of secular gravitational heating (see e.g. Aumer & Binney 2009; Aumer et al. 2016a). The shape of the relation between the age and $\sigma_{\rm z,birth}$ is also similar to the "plaw" model used in Aumer & Binney (2017). For this model they used observations from Wisnioski et al. (2015) (see section 1.2), who found that high redshift galaxies are observed to be more turbulent. This tells us that our results are in line with observations of high-redshift galaxies.

In figure 3.11, we now include the observation data of Mackereth et al. (2019) to our the age-birth vertical velocity dispersion relation. From this it is clear that the observational data has a higher vertical velocity dispersion than we would expect with only turbulent heating.

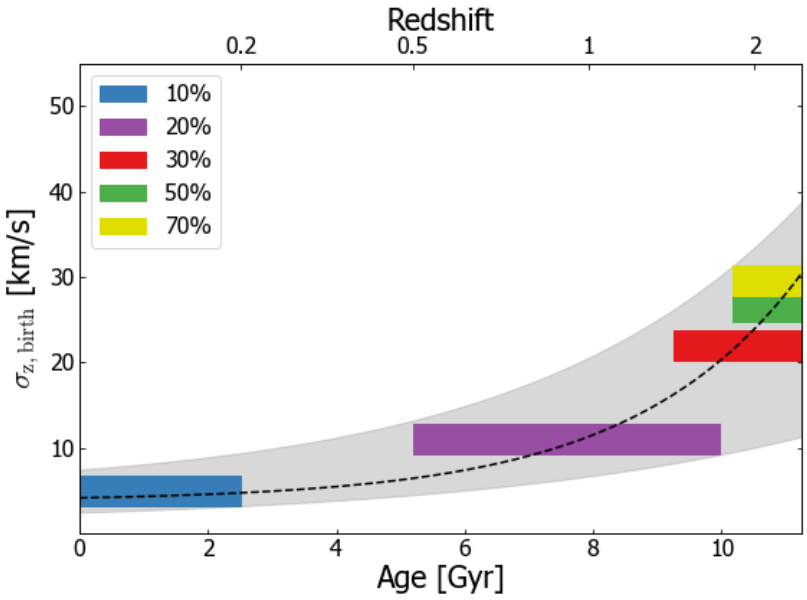

Figure 3.10: Age-birth velocity dispersion relation for the simulated galaxies. The redshift of each simulation is determined using figure 3.3. The center of the bar is located at the $\sigma_{z,birth}$ at 300 Myr, the width of the bar represent the spread of values as shown in figure 3.4. The dashed line is the best non-linear least squares fit through the data using $\sigma_{z,birth} \propto \exp(t)$, the gray shaded area indicates the outer edge of the fit.

There are two ways to explain this difference: (1) the different gas fraction regimes should have happened later then we expected (figure 3.11a) or (2) there is another type of heating that plays a role in the AVR (figure 3.11b). The first option seems unlikely, because in figure 3.5 we found that it is impossible for a thin disk to form for $f_g \geq 30\%$. If the Milky Way has a significantly higher gas fraction at a late cosmic time, as shown in figure 3.11a, the thin disk could only be a maximum ~ 5 Gyr old. From the observational data from Mackereth et al. (2019) in section 1.1.1 we know that this in disagreement with observational findings, because they observed thin disk stars with ages between 1.8 and 6.2 Gyr.

We hence conclude that the velocity dispersion imprinted at birth by the turbulent ISM and violent clump scattering is insufficient for explaining the observed AVR. In figure 3.11b we illustrate the excess secular heating required for our models to match the observations. According to theory (see section 1.1.1 for more details) several physical processes work together to establish the AVR, like the scattering of stars and GMCs (Spitzer & Schwarzschild 1953; Lacey 1984). In the next section we will delve deeper into the second option and focus on the impact of secular heating on the AVR.

3.4.2 Age-velocity dispersion relation

In figure 3.12a we present fits using a non-linear least squares method to the observed AVR from Mackereth et al. (2019) using

$$\sigma(t) = \sigma_{10} \cdot \left(\frac{t}{10\ \text{Gyr}}\right)^{\beta}, \tag{3.2}$$

where σ_{10} is the vertical velocity dispersion at 10 Gyr, t is the age of the stars, and β describes the efficiency of stochastic acceleration. This parameterization was used by Aumer et al. (2016a) to approximate the AVRs and heating histories of their N-body simulations of growing disk galaxies. We note that no *single* power law can fit the data as shown. In fact, separate relations must be used for the thin and thick disk, with different power law indices respectively, as shown

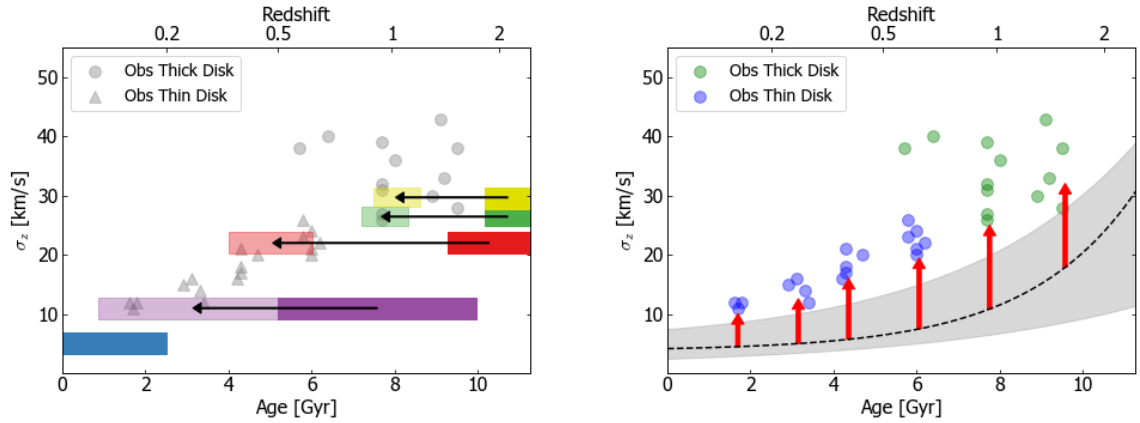

Figure 3.11: The $\sigma_{z,\text{birth}}$-age relation for each gas fraction from figure 3.10 with the observational data from Mackereth et al. (2019). In (a) we use the bars to indicate the location of the the different gas fractions and the arrows indicate where the gas fraction regimes have to move towards, to make the $\sigma_{z,\text{birth}}$ compatible with observations. In (b) the red arrows demonstrate the extra heating needed to be compatible to the observational data. The black line illustrates the best fit with the errror margins in gray (see figure 3.10)

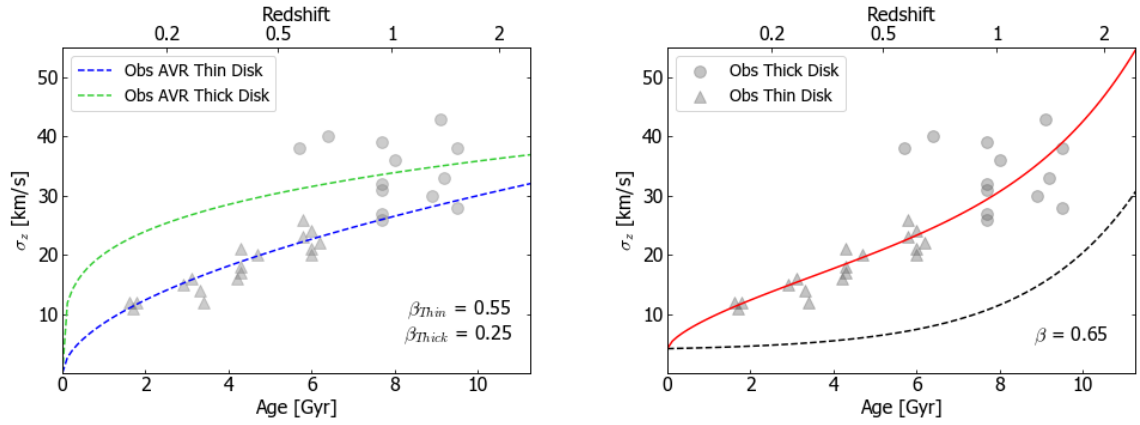

Figure 3.12: The age-velocity dispersion relation using observational data from Mackereth et al. (2019). Figure (a) uses a modified power law from Aumer et al. (2016a) (equation 3.2) to fit the observational data. At least two separate relations for the thick and thin disk, with different values of β is required to match the data. Figure (b) fits equation 3.3 to the same observational data shown by the red line. This new function includes both secular and turbulent heating (black line) and gives us a relation that better matches the thick and thin disk together.

in the figure. Taken at its face value, this scenario implies a clear overlap in time for the formation of the thick and thin disk at 6-10 Gyr. Such a formation scenario does not necessarily occur co-spatially due to the effect of the radial mixing of stars. In fact, this picture is supported by recent observational work by Beraldo e Silva et al. (2021) who found that the eccentricity of old stars can be used as evidence for an early co-formation of the thin and thick disk (see section 1.1.2). Furthermore, theoretical work by Agertz et al. (2021) found that the chemically defined thin and thick disk can be co-eval due to the way in which the disk assembles (see section 1.1).

This parameterization does not yet include the turbulent heating as shown in figure 3.10. To incorporate the heating of the turbulent ISM, we transform equation 3.2 to include both the

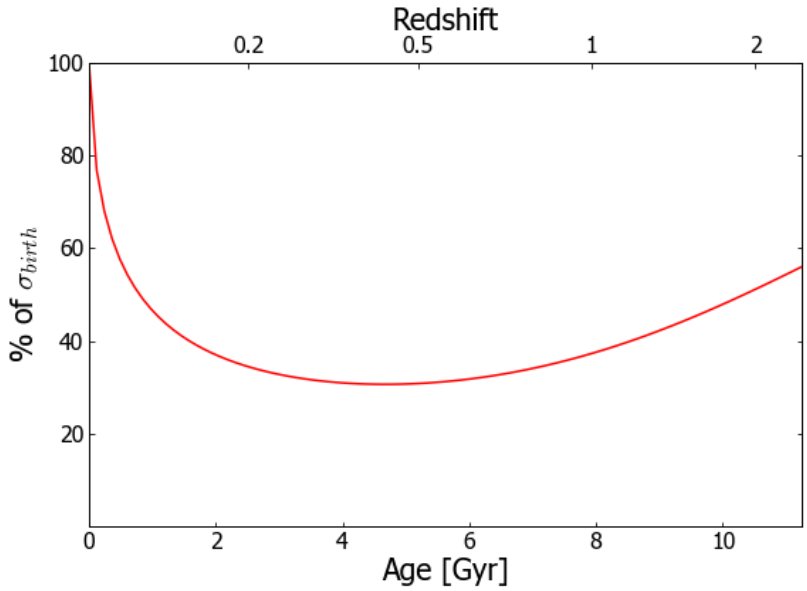

Figure 3.13: The percentage of σ_{birth} responsible for total heating of the system. We determine this by using the red line (total heating) and black dashed line (turbulent heating) shown in figure 3.12b.

turbulent and secular heating

$$\sigma(t) = \sigma_{\text{birth}} + (\sigma_{10} - \sigma_{\text{birth},10}) \cdot \left(\frac{t}{10\ \text{Gyr}}\right)^{\beta}, \tag{3.3}$$

where σ_{birth} is the turbulent heating as a function of time and $\sigma_{\text{birth},10}$ is the turbulent heating at 10 Gyr. In figure 3.12b we fitted this function to the observational data of Mackereth et al. (2019) using the non-linear least squares method. In contrast to figure 3.12a using equation 3.2, adding in the turbulent heating to the parameterization provides a much better match that represents the thick and thin disk together. We note that this does *not* preclude the co-eval formation scenario discussed above.

It is possible that different parts of the galaxy experienced a wide range of turbulent heating levels, i.e. that stars born at the same time were born in different gas fraction regimes. This would mean that some stars are still not well represented by the suggested function. This could explain some of the outliers we see in figure 3.12b. This indicates that we observe a mixture of stars with different birth environments, but formed co-evally in the Solar neighbourhood.

Figure 3.13 shows the percentage of σ_{birth} responsible for total heating of the system. In this figure it is shown that the turbulent heating is always responsible for at least 30% of the total heating. The turbulent heating is most important for very young stars, that have not had the time yet to be heated by secular heating, and for the older stars that were born in more gas-rich regimes and thus had a higher vertical velocity dispersion to begin with. To conclude, we find that turbulent gas motions imprint a significant velocity dispersion in early formed stellar populations, accounting for as much as 50% of the vertical kinematics in the old stars.

3.4.3 Constraining the ISM during disk formation

As discussed in section 3.3.2, it makes sense that none of the gas fraction runs correspond to the observational data of Li et al. (2018) in figure 3.9. The Milky Way has formed stars during a wide range of gas fractions meaning stars observed in the Solar neighbourhood will carry a mixture of environment imprints. By combining the data from the simulated galaxies at different gas fractions and the observational data, we probe which environments, in terms of gas fraction,

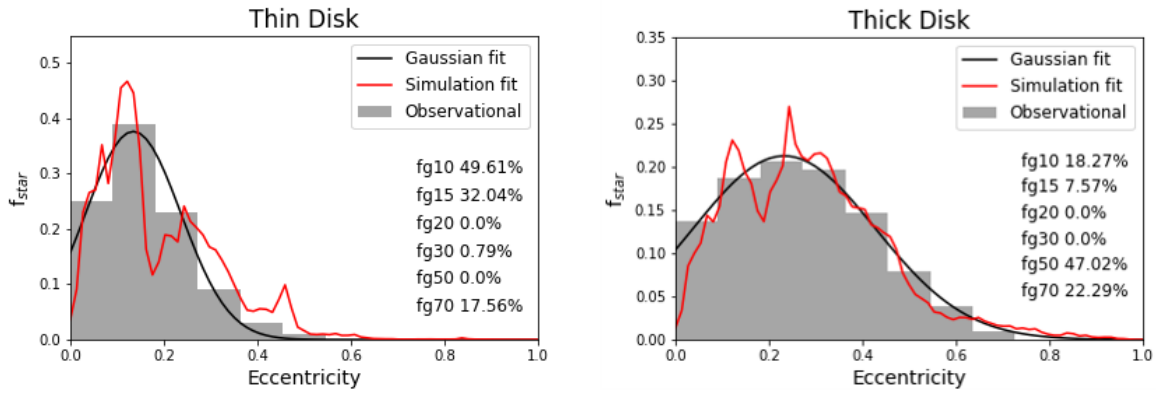

(a) **(b)**

Figure 3.14: The eccentricity distribution from observations in the solar neighbourhood by Li et al. (2018) of the thin (left) and thick (right) disk. The Gaussian fit on the observations is shown by the black line. The red line shows the best fit using equation 3.4 using the different gas fraction simulation.

	SFR $[M_\odot\ yr^{-1}]$	Redshift	Lookback time [Gyr]	$\sigma_{z,birth}$ $[km\ s^{-1}]$	Formation (MW Snhb)	
					Thin Disk	Thick Disk
fg10	1 ± 0.25	0.0 - 0.2	0 - 2.5	5	49.61%	18.27%
fg15	4 ± 0.5	0.5 - 1.7	5.1- 9.9	10	32.03%	7.57%
fg20	5 ± 0.8	0.5 - 1.7	5.1 -9.9	11	0.0%	0.0%
fg30	15 ± 2	1.4 - 2.6	9.1 - 11.2	23	0.79%	0.0%
fg50	25 ± 5	1.8 - 2.6	10.1 - 11.2	33	0.0%	47.02%
fg70	50 ± 10	1.8 - 2.6	10.1 - 11.2	29.5	17.56%	22.29%

Table 3.1: Properties of the different gas fraction runs. The redshift is determined using the implied SFR - redshift relation given by van Dokkum et al. (2013), the SFR and $\sigma_{z,birth}$ are estimated at 300 Myr for the runs.

were present when the thick and thin disk formed. To achieve this, we fit the observational data using a non-linear least squares method with the simulated data[4] (as shown in figure 3.14) written in the form of

$$f_{star} = a \cdot e_{fg10} + b \cdot e_{fg15} + c \cdot e_{fg20} + d \cdot e_{fg30} + e \cdot e_{fg50} + f \cdot e_{fg70} \tag{3.4}$$

The resulting best fits are shown in figure 3.14a and 3.14b respectively. The idea of this fit is that we take the eccentricity distribution of each simulation, $e_{fg..}$, and determine for how many percent the simulation is responsible for the Gaussian fit on the observation data of Li et al. (2018). The total sum of $a + b + c + d + e + f = 1$.

This shows us that most of the thick disk stars (figure 3.14b) are formed in a gas-rich (>50%) environment, whereas in the thin disk (figure 3.14a) most of the stars are formed in a gas-poor (<20%) environment. However, both the disks include a gas-rich and -poor regime, there is significant overlap in the gas fractions. For example both the thin and thick disk include stars from the $f_g = 70\%$ simulation. As discussed in section 1.1.2, Beraldo e Silva et al. (2021) used the eccentricity of old stars as evidence for an early co-formation of the thin and thick disk. In our case, both the thick and thin disk include stars from the higher gas fraction regime, this would correspond to the theory of early co-formation. Nevertheless, it is important to note that our model is not unique and that cosmological aspects like mergers will most likely alter the

[4]To create a more accurate fit we ran an extra simulation with a gas fraction of 15%.

contributions of different epochs. Radial migration could also have an effect as stars of different regions would end up in the Milky Way Solar neighbourhood.

Table 3.1 summarizes the findings of this section. From this data we can approximately infer when the thick disk and thin disk formed. We find that $\sim 70\%$ of the thick disk formed around 10 Gyr ago in environments with $f_g \gtrsim 50\%$. In contrast, we infer that $\sim 80\%$ of the thin disk formed in the past $\sim 9-10$ Gyr. We re-emphasize that the thick disk has a significant fraction of stars on near circular orbits, indicating they have formed in a lower gas fraction environment, and vice versa for the thin disk. This indicates a co-eval formation scenario for the thin and thick disk with different star forming environments across the entire Galaxy. Further limitations and drawbacks of our study, and how they affect our conclusions, will be discussed in section 4.2.

3.5 Summary

Chapter 3

- The simulations with different gas fractions are approximate representative of high redshift Milky Way analogues (20%,30%, 50%, 70%) and the current epoch of the Milky Way (10%). Their corresponding cosmic times are found by comparing observationally inferred star formation histories from van Dokkum et al. (2013) to the star formation rate of the different simulations.
- Stars born in disk galaxies with higher gas fractions feature higher vertical velocity dispersions. Simulations with a gas fraction of $\geq 50\%$ generate stellar velocity dispersions ~ 30 km/s in newly born stars.
- Stars born in disk galaxies with a 10% gas fraction feature stars on mostly circular orbits. As the gas fraction is increased, more stars end up on more eccentric orbits. The eccentricity distribution of $f_g = 30\%$, 50% and 70% are characterised by mean eccentricities of ~ 0.5, with more uniform distributions found for the highest gas fractions simulations.
- By comparing our simulations to Milky Way observations we infer that turbulent heating is a very important part of the total heating of a system, being responsible for at least 30% of the heating at all time, and $\sim 50\%$ for stars formed at $z \sim 2$.

Chapter 4

Discussion

In this work, we investigate the imprints of the stellar birth environment in the early Universe on the formation of the thin and thick disk. We find that the highly turbulent and fragmented state that we observe in high redshift galaxies imprints thick disk properties during star formation. This has a significant impact on the properties of the stars, by rapidly increasing their birth velocity dispersion and orbital eccentricities.

We discussed in chapter 1 that the thick disk stars are in general more radially compact, older, kinematically hotter than thin disk stars and feature a wide range of orbital eccentricities, while thin disk stars are better characterised by close to circular orbits (Holmberg et al. 2009; Schönrich & Binney 2009b; Bovy et al. 2012; Li et al. 2018; Mackereth et al. 2019; Feuillet et al. 2019, to name a few). In this work, we carry out state-of-the-art hydro+N-body simulations of entire galactic disks with gas fractions from 10 to 70 percent. We have shown that when we try to form the thick and thin disk only using turbulent heating, the thick disk is still kinematically hotter and features a larger range of orbital eccentricities than the thin disk. Having established the impact of the turbulent heating induced by the different gas fractions on vertical and radial stellar kinematics, we next turn to an analysis of the implications of our results for the evolution of the Milky Way. For this we use the AVR model of Aumer et al. (2016a), Gaia and APOGEE observations discussed in Mackereth et al. (2019) for velocity dispersions and Li et al. (2018) for eccentricities. We find that an initial gas fraction of 30% approximately marks a transition between the thin and thick disk. As such, the turbulent and fragmented interstellar medium at higher gas fractions acts as a "barrier" against thin disk formation. By creating a model including secular and turbulent heating that both matches thin and thick disk observations, we discover that the early turbulent heating is being responsible for at least 30% of the heating at all times. As expected, the thick disk was formed mostly in a high gas fraction regime, whereas the thin disk was mostly formed in a low gas fraction regime. Beraldo e Silva et al. (2021) used the eccentricity of old stars as evidence for an early co-formation of the thin and thick disk. In our case, both the thick and thin disk include stars from the higher gas fraction regime, this would correspond to the theory of early co-formation explored.

4.1 Comparison to literature

If we compare our work to recent work studying the age-velocity dispersion relation, we see that a lot of work focuses on secular heating and/or the impact of mergers or other influences from outside the Galaxy (see e.g. Bournaud et al. 2009; Aumer et al. 2016a). In our work we find the importance of turbulent heating and that a lot of the thin and thick disk properties can be explained by in-situ scenarios. In this section we discuss some of the more recent works.

Aumer et al. (2016a) concluded that for the expected disk mass and dark halo structure, combined GMC and spiral/bar heating can explain the AVR of the Galactic thin disk by analysing the heating of stellar disks in N-body simulations of growing disk galaxies. Similarly, Grand

et al. (2016) demonstrates that a bar is the dominant heating mechanism in most cases, whereas spiral arms, radial migration, and adiabatic heating from mid-plane density growth are all sub-dominant. In our work, the simulations of disk galaxies do not include a bar. We have found that for the thin disk, secular heating is more important than turbulent heating for stars born at least 1 Gyr ago (see figure 3.13), however that to create a full picture on the heating of the disk using in-situ mechanism we believe one needs to include both secular and turbulent heating. We have found that the turbulent heating is responsible for 40-30% of the total heating in the thin disk and 35% - 55% for the thick disk.

Aumer et al. wrote 4 papers using the same N-body models of growing disk galaxies. In paper 1 and 2 (Aumer et al. 2016b,a) they were missing models that both could explain the formation of the thick and thin disk. They concluded that the thick disk requires additional sources of heat early in the disk's life, prior to the onset of thin-disk formation, but that the thin disk can be explained by combined GMC and spiral heating. Paper 1 (Aumer et al. 2016b) concludes that the thick disk must have been heated prior to formation of the thin disk, our results agree with the fact that preheating from the ISM is required. In paper 3, Aumer & Binney (2017) introduced a new technique where the thick disk stars are created ad-hoc. The young stellar populations are assigned birth velocity dispersions which depend on the time they were born. The relation between the birth velocity dispersion and age we find in figure 3.10, is in-agreement with their "plaw" model. The model is based on the observations done by Wisnioski et al. (2015), who found that high redshift galaxies are observed to be more turbulent.

Martig et al. (2014) followed a different approach than Aumer et al., studying the AVR in a sample of simulated disk galaxies that all first undergo an active phase of mergers at high redshift. They found that the slope of the AVR is not imprinted at birth, but is due to heating over time. They have not been able to pin down the exact mechanisms responsible for that heating, however they state that radial migration is not one of them. Their results are in agreement with the observational findings in the Milky Way Solar neighbourhood of Holmberg et al. (2009). In contrast, we have found that the turbulent heating at birth cannot be neglected and plays a big role in the slope of the AVR. In our work, we include observational data from Gaia and APOGEE from stars between 6 and 11 kpc (Mackereth et al. 2019) to compare the AVR. The differences between our samples could explain why we have different findings. Another explanation could be the different ways the star formation is modeled. A number of simulators have examined the origin of the AVR and the formation of Galaxy thin and thick disks, from which one trend that has become clear, the results can be strongly dependent on the star formation parameters, which are commonly limited by the simulation resolution (House et al. 2011; Bird et al. 2013; Martig et al. 2014; Kumamoto et al. 2017). In contrast to Martig et al. (2014), Bird et al. (2013) finds that the trends of spatial structure and kinematics with stellar age are largely imprinted at birth, or immediately thereafter. Our work agrees with the findings of Bird et al. (2013) that a big part of the kinematics of the stars are imprinted at birth.

While preparing this thesis, Bird et al. (2021) found a nearly identical AVR to that of the analogous Solar neighborhood measurement in the Milky Way using high resolution cosmological simulations. A crucial element of their success is the simulation's dynamically cold multi-phase ISM, which allows recently formed stars to have a low velocity dispersion and older stars being born kinematically hotter. Their $\sigma_{\mathrm{z,birth}}$-age relation is in line with our findings. Their simulation is just one simulation of a Milky Way-mass galaxy, so it is not yet clear if the results will persist in additional simulations. It had a very quiescent merger history over the past 10 Gyr, so mergers are unlikely to be a major source of heating in this particular galaxy simulation.

4.2 Limitations

We carried out state-of-the-art hydrodynamical+N-body in-situ simulations of entire galactic disks with gas fractions from 10 to 70 percent, and compared them to observational data from

APOGEE and Gaia used by Mackereth et al. (2019) and Li et al. (2018). A potential lack of realism is connected to the disk size, which stays the same for all the different simulations at different gas fractions. It is critical to note that the disk sizes in the earliest epochs were smaller than adopted in our work, as is shown for example by Paulino-Afonso et al. (2017).

Furthermore, the initial conditions of our simulations are idealized, and the extent of the gas disk may not be fully captured. In contrast to many other studies (e.g. Bird et al. 2013; Martig et al. 2014; Bird et al. 2021), our work does not include any cosmology in the simulations. This gives us a moderately good grasp of the physics that determines the size, mass and abundance, noted as the fundamental characteristics of galaxies, but we miss the physics that will help us further determining the internal structure and evolution of galaxies (Naab & Ostriker 2017). To get a more realistic view on the turbulent heating of the system we could include the radiation fields, the baryonic gas as well as the energy, processed interstellar matter and momentum input from the stars and massive black holes. This all shows that our model is simplified.

In our last section of chapter 3, we discussed the implications for the evolution of the Milky Way, which was very exploratory work. We started by creating a model for the heating of the Milky Way using only turbulent heating, For this we determine the redshift of our simulations by eye using the van Dokkum et al. (2013) data points. This gives a high uncertainty and large ranges of possible redshift for the regimes.

Lastly, to constrain the ISM during disk formation, we only used observations in the Milky Way Solar neighbourhood, which is presumably not representative to the eccentricity distribution of the whole Milky Way. It is very likely that different parts, like the bulge and the outer edge of the thick disk, of the Galaxy experienced a wide range of turbulent heating levels. This has as a result that stars born at the same time may have been born in different gas fraction regimes and thus different regions will have different eccentricity distributions. Another reason for the fact that the Solar neighbourhood distribution will be different than that of the other sections of the Milky Way is the radial mixing of stars, something we do not explore in this work. The stars closer to the centre of the Milky Way will have a bigger eccentricity range as shown in section 3.3.1. The gas is less turbulent and fragmented at the outskirts of the disk and stars closer to the galactic center will have a shorter orbital time and thus have a higher probability to get heated up. Therefore stars from another region of the Milky Way are not representative to the birth conditions of the stars formed in the Solar neighbourhood. This makes the connection we made with redshift and formation of thin and thick disk using eccentricity in section 3.4.3 less correct.

4.3 Outlook

We have simulated different epochs of the Milky Ways by only changing the gas fraction. As with any study, one can always strive for improvement in the adopted methodology and in our case this could mean implementing more cosmology into the system and include a changing disk size depending on the gas fraction. However, this will make us lose the benefits of a controlled experiment in the way we currently have. Therefore a more tandem approach makes sense, by understanding how the thin and thick disks form both via isolated setups and full cosmological simulations. Future work using these cosmological simulations would be especially interesting to control the merger history an being able to link this to the conclusions of this work.

Furthermore, to get more realistic epochs of the Milky Way, we should account for the galaxy growth in future work. We could do this by for example using a cooling halo (see e.g. Khoperskov et al. 2021). This is important, because Agertz et al. (2021) showed us that the galaxy grows inside-out and evolves secularly in the last $\sim$ 8 Gyr. This galaxy formation scenario, is the notion that young stellar populations reside in a thin as well as a radially more extended disk (e.g. Bird et al. 2013). So adopting more realistic epochs of the Milky Way by taking into account the galaxy growth, can be used to connect the kinematics to a way in which the disk is

growing inside out.

We compare our simulations to observations. These observations (in our work, we use Mackereth et al. 2019; Li et al. 2018) use the chemical definition of the thick an thin disk. In general, chemical, spatial and kinematical properies of stars teaches us different things about the galaxy (see e.g. Agertz et al. 2021; Renaud et al. 2021). For future work, we should thus try to compare the chemical charateristics in our simulations to the observations. To get the chemical properties of the stars in our simulations, it requires Hubble time of modeling in a cosmological context.

Chapter 5

Conclusion

In this work, we investigate the imprints of the birth environment in which stars formed in the early Universe on the formation of the thin and thick disk of the Milky Way. Our findings are summarized as follows:

- Stars born in disk galaxies with high gas fractions feature high vertical velocity dispersions. Simulations with a gas fraction of $\geq 50\%$ generate stellar velocity dispersions ~ 30 km/s already at star formation, well above the observed kinematics in the Milky Way's thin disk. (Mackereth et al. 2019). In contrast, simulations with a gas fraction of $\lesssim 20\%$ form stars with velocity dispersions $\lesssim 10$ km/s, in line with young stars in the Milky Way's thin disk. We find that an initial gas fraction of 30% approximately marks a transition between the thin and thick disk. As such, the turbulent and fragmented interstellar medium at higher gas fractions act as a 'barrier' against thin disk formation.

- We find that orbital eccentricities of young stars depend sensitively to the gas fraction of the simulated galaxies. Stars born in disk galaxies with a 10% gas fraction feature stars on mostly circular orbits, with a mean orbital eccentricity less than 0.2. As the gas fraction is increased, more stars end up on more eccentric orbits. We find that once the gas fraction is $\gtrsim 30\%$, all eccentricity distributions are characterised by mean eccentricities of ~ 0.5, with more uniform distributions found for the highest gas fractions simulations ($f_{\mathrm{g}} = 50\%$ and 70%). This 'saturation' effect above $f_{\mathrm{g}} = 30\%$ is in line with what was identified for the vertical velocity dispersions.

- By mapping the estimated redshift range of each simulation to the corresponding birth velocity dispersion, we make a direct comparison to the Milky Way's AVR from Mackereth et al. (2019). This allows us to approximate the roles played by slow secular heating and turbulent heating imprinted at star formation. We find that turbulent heating is a non-negligible part of the total stellar heating in a disk galaxy, being responsible for at least 30% of the heating at all time, and as much as 50% over 10 Gyr ago.

- By combining the simulated eccentricity distributions with observational data of Li et al. (2018), we infer the gas fractions and formation epochs of the Milky Way's chemically defined thick and thin disks. We find that $\sim 70\%$ of the thick disk formed in a high gas fraction ($\geq 50\%$) environment, whereas 80% of the thin disk was formed in a low gas fraction ($\leq 20\%$) environment. It is noteworthy that both disks require some contribution of gas-rich and -poor regimes to fully characterise their eccentricity distributions. This notion is compatible with a thin/thick disc co-formation scenario (e.g. Agertz et al. 2021; Renaud et al. 2021; Beraldo e Silva et al. 2021) in which a range of ISM conditions existed simultaneously, with radial migration later mixing stars across the galaxy.

Acknowledgement

First, and foremost, I would like to thank my supervisor, Oscar Agertz, for his amazing guidance at every stage of the research project and the insightful comments and suggestions.

In addition, I would like to express my gratitude to my parents, who morally and physically supported me even though I am positive none of them have any idea what I was usually talking about (prove me wrong). Special thanks go to Besi Sedijaj for being my rubber duck during all the debugging. And finally, I could not have completed this project without the support of my friends, Manon Maarseveen and Lesley van de Pavert, who voluntarily checked the (mostly Dutch) grammar of my report.

Bibliography

Abadi, M. G., Navarro, J. F., Steinmetz, M., & Eke, V. R. 2003, ApJ, 597, 21

Agertz, O. & Kravtsov, A. V. 2015, ApJ, 804, 18

Agertz, O., Kravtsov, A. V., Leitner, S. N., & Gnedin, N. Y. 2013, ApJ, 770, 25

Agertz, O., Moore, B., Stadel, J., et al. 2007, MNRAS, 380, 963

Agertz, O., Renaud, F., Feltzing, S., et al. 2021, MNRAS, 503, 5826

Agertz, O., Romeo, A. B., & Grisdale, K. 2015, MNRAS, 449, 2156

Agertz, O., Teyssier, R., & Moore, B. 2011, MNRAS, 410, 1391

Aumer, M. & Binney, J. 2017, MNRAS, 470, 2113

Aumer, M., Binney, J., & Schönrich, R. 2016a, MNRAS, 462, 1697

Aumer, M., Binney, J., & Schönrich, R. 2016b, MNRAS, 459, 3326

Aumer, M., Binney, J., & Schönrich, R. 2017, MNRAS, 470, 3685

Aumer, M. & Binney, J. J. 2009, MNRAS, 397, 1286

Barnes, A. T., Longmore, S. N., Battersby, C., et al. 2017, MNRAS, 469, 2263

Bensby, T., Feltzing, S., & Oey, M. S. 2014, A&A, 562, A71

Beraldo e Silva, L., Debattista, V. P., Nidever, D., Amarante, J. A. S., & Garver, B. 2021, MNRAS, 502, 260

Bird, J. C., Kazantzidis, S., Weinberg, D. H., et al. 2013, ApJ, 773, 43

Bird, J. C., Loebman, S. R., Weinberg, D. H., et al. 2021, MNRAS, 503, 1815

Bland-Hawthorn, J. & Gerhard, O. 2016, ARA&A, 54, 529

Bournaud, F., Elmegreen, B. G., & Martig, M. 2009, ApJL, 707, L1

Bovy, J., Rix, H.-W., Liu, C., et al. 2012, ApJ, 753, 148

Bovy, J., Rix, H.-W., Schlafly, E. F., et al. 2016, ApJ, 823, 30

Brook, C. B., Gibson, B. K., Martel, H., & Kawata, D. 2005, ApJ, 630, 298

Brook, C. B., Stinson, G. S., Gibson, B. K., et al. 2012, MNRAS, 426, 690

Buck, T., Obreja, A., Macciò, A. V., et al. 2020, MNRAS, 491, 3461

Bullock, J. S., Kolatt, T. S., Sigad, Y., et al. 2001, MNRAS, 321, 559

Chabrier, G. 2003, PASP, 115, 763

Clarke, A. J., Debattista, V. P., Nidever, D. L., et al. 2019, MNRAS, 484, 3476

Courteau, S., Dutton, A. A., van den Bosch, F. C., et al. 2007, ApJ, 671, 203

de Rossi, M. E., Tissera, P. B., De Lucia, G., & Kauffmann, G. 2009, MNRAS, 395, 210

Debattista, V. P., Gonzalez, O. A., Sanderson, R. E., et al. 2019, MNRAS, 485, 5073

Dessauges-Zavadsky, M., Richard, J., Combes, F., et al. 2019, Nature Astronomy, 3, 1115

Dierickx, M., Klement, R., Rix, H.-W., & Liu, C. 2010, ApJL, 725, L186

Dutton, A. A., Conroy, C., van den Bosch, F. C., et al. 2011, MNRAS, 416, 322

Ejdetjärn, T. 2019, Investigating Gas Turbulence in Galactic Discs, student Paper

Elmegreen, D. M., Elmegreen, B. G., Marcus, M. T., et al. 2009, ApJ, 701, 306

Feuillet, D. K., Frankel, N., Lind, K., et al. 2019, MNRAS, 489, 1742

Freeman, K. & Bland-Hawthorn, J. 2002, ARA&A, 40, 487

Gilmore, G. & Reid, N. 1983, MNRAS, 202, 1025

Grand, R. J. J., Springel, V., Gómez, F. A., et al. 2016, MNRAS, 459, 199

Grisdale, K., Agertz, O., Renaud, F., & Romeo, A. B. 2018, MNRAS, 479, 3167

Grisdale, K., Agertz, O., Renaud, F., et al. 2019, MNRAS, 486, 5482

Grisdale, K., Agertz, O., Romeo, A. B., Renaud, F., & Read, J. I. 2017, MNRAS, 466, 1093

Guillet, T. & Teyssier, R. 2011, Journal of Computational Physics, 230, 4756

Hayden, M. R., Bovy, J., Holtzman, J. A., et al. 2015, ApJ, 808, 132

Hernquist, L. 1990, ApJ, 356, 359

Hernquist, L. 1993, ApJS, 86, 389

Hockney, R. W. & Eastwood, J. W. 1981, Computer Simulation Using Particles

Holmberg, J., Nordström, B., & Andersen, J. 2009, A&A, 501, 941

House, E. L., Brook, C. B., Gibson, B. K., et al. 2011, MNRAS, 415, 2652

Jurić, M., Ivezić, Ž., Brooks, A., et al. 2008, ApJ, 673, 864

Khoperskov, S., Haywood, M., Snaith, O., et al. 2021, MNRAS, 501, 5176

Kim, C.-G. & Ostriker, E. C. 2015, ApJ, 802, 99

Kim, J.-h., Abel, T., Agertz, O., et al. 2014, ApJS, 210, 14

Kim, J.-h., Agertz, O., Teyssier, R., et al. 2016, ApJ, 833, 202

Kormendy, J. & Barentine, J. C. 2010, ApJL, 715, L176

Kumamoto, J., Baba, J., & Saitoh, T. R. 2017, PASJ, 69, 32

Lacey, C. G. 1984, MNRAS, 208, 687

Lee, E. J., Miville-Deschênes, M.-A., & Murray, N. W. 2016, ApJ, 833, 229

Li, C., Zhao, G., Zhai, M., & Jia, Y. 2018, ApJ, 860, 53

Mackereth, J. T., Bovy, J., Leung, H. W., et al. 2019, MNRAS, 489, 176

Martig, M., Minchev, I., & Flynn, C. 2014, MNRAS, 443, 2452

Martizzi, D., Faucher-Giguère, C.-A., & Quataert, E. 2015, MNRAS, 450, 504

Minchev, I. & Quillen, A. C. 2006, MNRAS, 368, 623

Naab, T. & Ostriker, J. P. 2017, ARA&A, 55, 59

Navarro, J. F., Frenk, C. S., & White, S. D. M. 1996, ApJ, 462, 563

Nordström, B., Mayor, M., Andersen, J., et al. 2004, A&A, 418, 989

Paulino-Afonso, A., Sobral, D., Buitrago, F., & Afonso, J. 2017, MNRAS, 465, 2717

Pillepich, A., Nelson, D., Springel, V., et al. 2019, MNRAS, 490, 3196

Quinn, P. J., Hernquist, L., & Fullagar, D. P. 1993, ApJ, 403, 74

Recio-Blanco, A., de Laverny, P., Kordopatis, G., et al. 2014, A&A, 567, A5

Renaud, F., Agertz, O., Read, J. I., et al. 2021, MNRAS, 503, 5846

Saintonge, A., Lutz, D., Genzel, R., et al. 2013, ApJ, 778, 2

Sales, L. V., Helmi, A., Abadi, M. G., et al. 2009, MNRAS, 400, L61

Santini, P., Maiolino, R., Magnelli, B., et al. 2014, A&A, 562, A30

Schönrich, R. & Binney, J. 2009a, MNRAS, 396, 203

Schönrich, R. & Binney, J. 2009b, MNRAS, 399, 1145

Sellwood, J. A. & Binney, J. J. 2002, MNRAS, 336, 785

Sellwood, J. A. & Carlberg, R. G. 1984, ApJ, 282, 61

Skelton, R. E., Whitaker, K. E., Momcheva, I. G., et al. 2014, ApJS, 214, 24

Spitzer, Lyman, J. & Schwarzschild, M. 1953, ApJ, 118, 106

Springel, V. 2000, MNRAS, 312, 859

Stewart, K. R., Bullock, J. S., Wechsler, R. H., Maller, A. H., & Zentner, A. R. 2008, ApJ, 683, 597

Teyssier, R. 2002, A&A, 385, 337

Turk, M. J., Smith, B. D., Oishi, J. S., et al. 2011, ApJS, 192, 9

van Dokkum, P. G., Leja, J., Nelson, E. J., et al. 2013, ApJL, 771, L35

Vera-Ciro, C., D'Onghia, E., Navarro, J., & Abadi, M. 2014, ApJ, 794, 173

Villalobos, Á. & Helmi, A. 2008, MNRAS, 391, 1806

Wisnioski, E., Förster Schreiber, N. M., Wuyts, S., et al. 2015, ApJ, 799, 209

Yoshii, Y. 1982, PASJ, 34, 365

List of Figures

List of Tables